ARTICLE

doi:10.1038/nature23909

Reversing behavioural abnormalities in mice exposed to maternal inflammation

Yeong Shin Yim[1,2], Ashley Park[1,2], Janet Berrios[1,2], Mathieu Lafourcade[1,2], Leila M. Pascual[1,2], Natalie Soares[1,2], Joo Yeon Kim[1,2], Sangdoo Kim[3], Hyunju Kim[3], Ari Waisman[4], Dan R. Littman[5,6], Ian R. Wickersham[1], Mark T. Harnett[1,2], Jun R. Huh[3]† & Gloria B. Choi[1,2]

Viral infection during pregnancy is correlated with increased frequency of neurodevelopmental disorders, and this is studied in mice prenatally subjected to maternal immune activation (MIA). We previously showed that maternal T helper 17 cells promote the development of cortical and behavioural abnormalities in MIA-affected offspring. Here we show that cortical abnormalities are preferentially localized to a region encompassing the dysgranular zone of the primary somatosensory cortex (S1DZ). Moreover, activation of pyramidal neurons in this cortical region was sufficient to induce MIA-associated behavioural phenotypes in wild-type animals, whereas reduction in neural activity rescued the behavioural abnormalities in MIA-affected offspring. Sociability and repetitive behavioural phenotypes could be selectively modulated according to the efferent targets of S1DZ. Our work identifies a cortical region primarily, if not exclusively, centred on the S1DZ as the major node of a neural network that mediates behavioural abnormalities observed in offspring exposed to maternal inflammation.

In humans, viral infection during pregnancy has been correlated with increased frequency of neurodevelopmental disorders in offspring[1–6], and this has been further modelled in mice[7–10]. We previously reported that the offspring from pregnant dams injected with polyinosinic:polycytidylic acid (poly(I:C)), which mimics viral infection, on embryonic day 12.5 (E12.5) exhibit behavioural abnormalities including abnormal communication, increased repetitive behaviours, and deficits in sociability[11]. In parallel to the behavioural abnormalities, we also observed that MIA-affected offspring display patches of disorganized cortical cytoarchitecture during embryonic development as well as in adulthood. The cortical phenotype was manifested as a loss of the cortical-layer-specific markers special AT-rich sequence-binding protein 2 (SATB2) and T-brain-1 (TBR1)[11]. Development of both MIA-associated behavioural phenotypes (MIA behaviours) and cortical patches were prevented by knocking out a key transcriptional regulator of T helper 17 cells, retinoic acid receptor-related orphan nuclear receptor gamma t (RORγt), in maternal T cells, or by inhibiting the activity of the effector cytokine IL-17a in pregnant dams[11]. These observations suggested that the maternal T helper 17 cell and IL-17a pathway is crucial for inducing MIA behaviours and for generating cortical patches in the offspring. However, whether the cortical phenotype is the underlying cause of the behavioural abnormalities in MIA offspring remained undetermined.

Characterization of cortical patches

We first wished to determine the distribution of cortical patches in the brains of adult MIA offspring by matching the locations of cortical regions that lack expression of SATB2 or TBR1 to those in a reference mouse brain atlas[12] (Fig. 1a). Cortical patches found in individual animals often retained similar mediolateral (ML) and dorsoventral (DV) coordinates through serial coronal sections, suggesting that many form a single continuous patch extending along the anteroposterior (AP) axis, rather than forming a series of independent patches (Extended Data Fig. 1a). Although cortical patches were detected at multiple locations throughout the cortex, they were prevalently observed in the primary somatosensory cortex (S1) at the AP level around 0.5 mm posterior to the bregma (AP = −0.5 mm; 90% of animals, $n = 10$) (Fig. 1b, Extended Data Fig. 1), as well as in the secondary motor cortex (M2) and other cortical regions, including the temporal association cortex (TeA) (80% and 40% of animals, respectively, $n = 10$) (Fig. 1b, Extended Data Fig. 1). Cortical patches were also most predominantly present in S1 with respect to both their number and sizes (Extended Data Fig. 1d), and often present in S1 unilaterally (60% of animals, $n = 10$). Furthermore, registration of cortical patches in individual MIA animals onto the same reference plane near AP level of −0.5 mm revealed that the cortical patches most consistently centred on S1DZ, a region of the primary somatosensory cortex that is morphologically characterized by the absence of a discernible 4th cortical layer and implicated in muscle- and joint-related functions (56% of animals, $n = 50$)[13–15] (Fig. 1c, Extended Data Fig. 2). On the basis of these results, we decided to carry out further analysis on S1 patches near AP −0.5 mm.

Deficits in interneuron function or dysregulation of neural activity in the somatosensory pathway have been previously associated with both genetic and environmental mouse models of neurodevelopmental disorders[16–18]. Similarly, we found that S1 cortical patches of MIA offspring display a specific loss of parvalbumin (PV) expression, which marks a class of interneurons derived from the medial ganglionic eminence[19]. This deficit in PV expression could reflect either the loss of PV protein expression or the loss of neurons marked by PV. We observed no significant differences in the expression of the neuron-specific marker NeuN[20] or of the vasoactive intestinal polypeptide (VIP)[19], which is expressed in interneurons derived from the caudal ganglionic eminence, between PBS control and MIA offspring (Fig. 1d, e, Extended Data Fig. 3a, b). To test whether the decrease in the number

[1]McGovern Institute for Brain Research, Massachusetts Institute of Technology, Cambridge, Massachusetts 02139, USA. [2]Department of Brain and Cognitive Sciences, Massachusetts Institute of Technology, Cambridge, Massachusetts 02139, USA. [3]Division of Infectious Diseases and Immunology and Program in Innate Immunity, Department of Medicine, University of Massachusetts Medical School, Worcester, Massachusetts 01605, USA. [4]Institute for Molecular Medicine, University Medical Center of the Johannes Gutenberg-University Mainz, Mainz, Germany. [5]Kimmel Center for Biology and Medicine of the Skirball Institute, New York University School of Medicine, New York, New York 10016, USA. [6]Howard Hughes Medical Institute, New York, New York 10016, USA. †Present address: Division of Immunology, Department of Microbiology and Immunobiology, Harvard Medical School, Boston, Massachusetts 02115, USA and Evergrande Center for Immunological Diseases, Harvard Medical School and Brigham and Women's Hospital, Boston, Massachusetts 02115, USA.

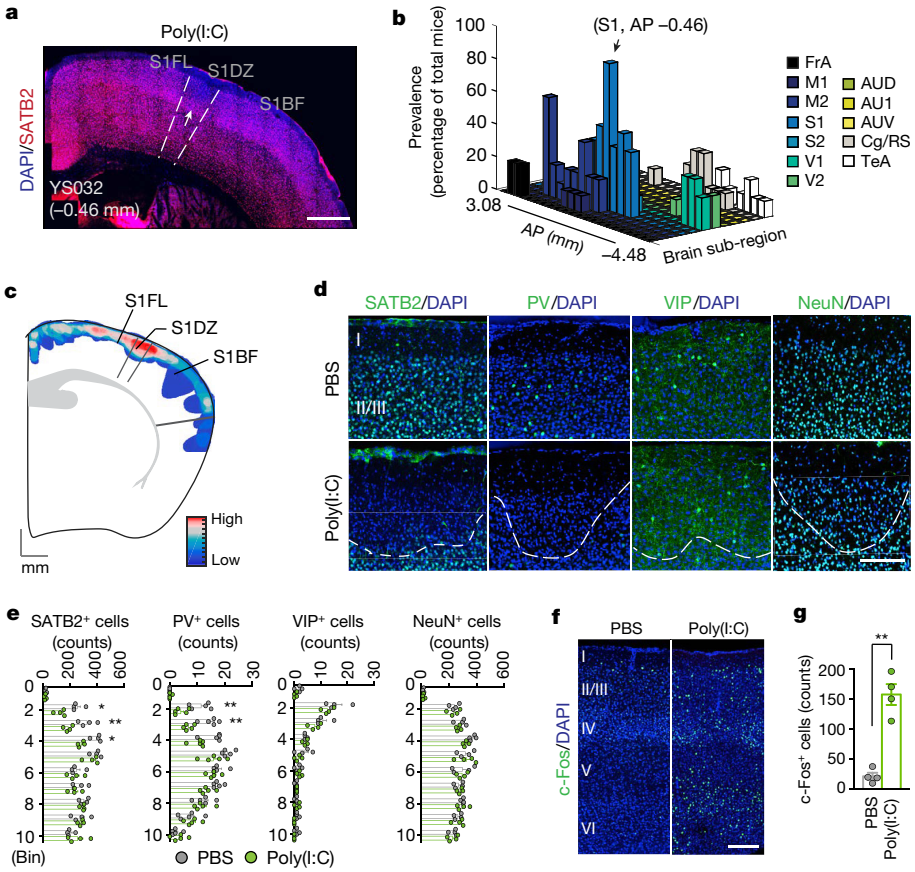

Figure 1 | Cortical patches observed in offspring of dams following MIA. a, Representative S1 image of adult MIA offspring. Arrow indicates cortical patch. Scale bar, 500 μm. **b**, Prevalence of cortical patches ($n = 10$ mice; 2 independent experiments) in MIA offspring. **c**, Superimposed image of cortical patches within AP 0.38 to −1.34 mm ($n = 50$ mice; 12 independent experiments). The mouse brain in this figure has been reproduced from ref. 12. Scale indicates frequencies of patches (high, red; low, blue). **d**, Representative images of S1. White dotted lines indicate boundary of cortical patches. Scale bar, 100 μm. **e**, Quantification of SATB2$^+$, PV$^+$, VIP$^+$, and NeuN$^+$ cells in S1 cortical patches ($n = 4$ PBS, 4 poly(I:C), 3 independent experiments for SATB2, VIP, and NeuN; $n = 5$ PBS, 5 poly(I:C), 3 independent experiments for PV). **f**, Representative images of c-Fos expression in S1. Scale bar, 100 μm. **g**, Quantification of c-Fos expression in S1 ($n = 4$ PBS, 4 poly(I:C); 3 independent experiments). $^*P < 0.05$, $^{**}P < 0.01$ calculated by two-way repeated measures ANOVA with Tukey (**e**) and two-tailed unpaired *t*-test (**g**). Graphs indicate mean ± s.e.m.

of PV$^+$ neurons results in a diminished inhibitory drive onto S1 pyramidal neurons, we used whole-cell patch-clamp recordings to measure the miniature inhibitory post-synaptic currents (mIPSCs) in S1 pyramidal neurons of PBS or MIA offspring. We indeed observed a reduction in frequency, but not amplitude, of mIPSCs (Extended Data Fig. 3c–h), paralleled by an increase in the number of S1 neurons that express c-Fos, a marker of neuronal activation (Fig. 1f, g, Extended Data Fig. 3i, j).

Cortical patches are predictive of MIA behaviours

To determine whether the development of MIA-associated behaviours and the appearance of cortical patches depend on the developmental timing at which MIA is induced, we injected poly(I:C) into pregnant dams at embryonic stages E12.5, E15.5 or E18.5, and assessed their offspring for MIA-associated behavioural phenotypes. We first examined the ability of the offspring to communicate by measuring the ultrasonic vocalization (USV) made by pups upon separation from their mothers at postnatal day 9 (P9). As previously reported[11], pups from pregnant dams injected with poly(I:C) at E12.5 (MIA offspring) emitted more USV calls than pups from PBS-injected dams (PBS offspring). However, such an increase was not observed in the offspring from dams injected with poly(I:C) at either E15.5 or E18.5 (Extended Data Fig. 4d–g). We also examined repetitive behaviours using the marble burying assay, natural inclination towards social targets with the sociability assay, and anxiety-related behaviours by measuring the time spent by adult MIA offspring at the centre of an open field (Extended Data Fig. 4a–c). For all behaviours, we observed deficits in the offspring when exposed to prenatal MIA at E12.5. Again, the behaviour of the offspring from mothers injected with poly(I:C) either at E15.5 or E18.5 were indistinguishable from those from PBS-injected mothers (Extended Data Fig. 4h–n), except for a reduction observed in the centre time during the open field assay for offspring exposed to MIA at E15.5. Importantly, chamber preference during habituation, the total interaction time during the sociability assay and the total distance travelled during the sociability and open field assays were similar among treatment groups, suggesting that differences in activity or arousal levels cannot explain the observed behavioural differences (Extended Data Fig. 4i, k, l, n). Our data strongly indicate that all behavioural abnormalities emerge from a discrete developmental stage, allowing us to examine whether the presence of cortical patches is predictive of MIA behavioural phenotypes. Indeed, we observed cortical patches in the S1 in 79% of offspring from dams injected with poly(I:C), but not PBS, at E12.5. Yet, cortical patches were seen only in 13% or none of the offspring when poly(I:C) was administered at E15.5 or E18.5, respectively (Fig. 2a). Thus, maternal inflammation induced at E15.5 and E18.5, unlike at E12.5, was ineffective in generating cortical patches and also failed to produce behavioural abnormalities in MIA offspring. Furthermore, the size of the S1 cortical patches correlated with the severity of behavioural phenotypes; the cortical patch sizes ranged from 0 (absence of the cortical patch) to 1 mm^2 and were positively correlated with the marble burying

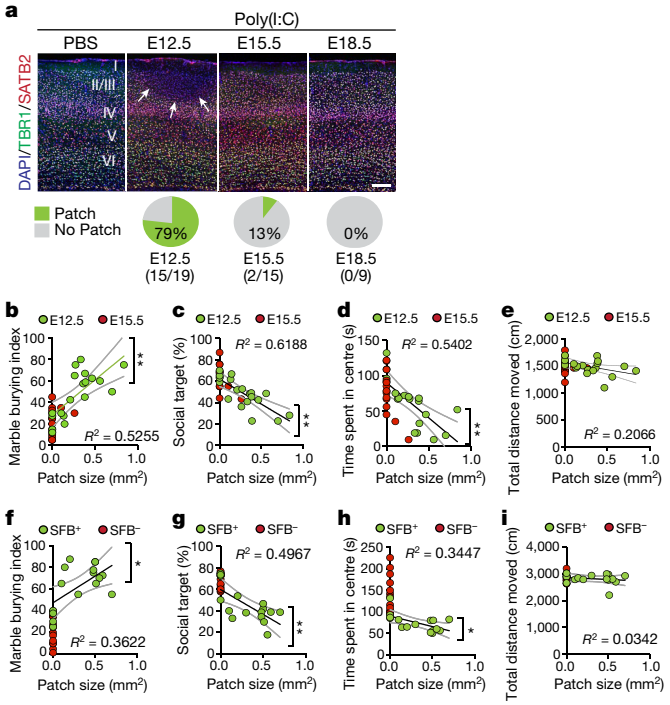

Figure 2 | The presence and size of cortical patches are predictive of MIA-induced behaviours and their severity in offspring. a, Top, representative S1 images of adult offspring from PBS- (E12.5; $n = 12$ mice, 7 independent experiments) and poly(I:C)-injected dams (E12.5, E15.5, E18.5; $n = 19$, 15, 9 mice, 7, 7, 5 independent experiments, respectively). Bottom, percentage of offspring with cortical patches in S1. Arrows indicate cortical patch. Scale bar, 100 μm. **b**–**i**, Cortical patch size plotted against behavioural severity in marble burying (**b**, **f**), sociability (**c**, **g**), and open field tests (**d**, **h**), and total distance moved during sociability (**e**, **i**) for offspring exposed to MIA at E12.5 and E15.5 (**b**–**e**) ($n = 19$, 15 mice, 7 independent experiments) or offspring from SFB^+ Taconic dams and SFB^- Jackson dams (**f**–**i**) ($n = 16$, 14 mice, 2 independent experiments). Green solid lines represent regression line; grey lines indicate 95% confidence intervals for E12.5 (**b**–**e**) or SFB^+ (**f**–**i**) groups. $^*P < 0.05$, $^{**}P < 0.01$ calculated by linear regression (**b**–**i**).

index, but negatively correlated with both sociability and time spent in the centre of an open field (Fig. 2b–d). The total distance travelled during the sociability assay was not affected by patch size (Fig. 2e). The size of cortical patches found outside of S1 also did not correlate with the severity of behavioural abnormalities (Extended Data Fig. 4o–q).

The accompanying paper by Kim *et al.*[21] demonstrates that a single species of bacteria—segmented filamentous bacteria (SFB)—present in C57BL/6 animals bred by Taconic Biosciences, but not in those from Jackson Laboratory, is required in mothers to induce behavioural abnormalities in MIA offspring[21]. All animals used in this study were also from mouse colonies carrying SFB. In accordance with our observation above, we found that the size of cortical patches in MIA offspring from SFB-present (SFB^+) dams was highly correlated with the severity of the behavioural phenotypes of the offspring, but not with the total distance travelled during the behavioural assay (Fig. 2f–i). On the other hand, offspring from SFB-absent (SFB^-), MIA-exposed mothers did not exhibit S1 cortical patches.

We previously showed that recombinant IL-17a injected into the ventricles of the developing brain requires intact IL-17 receptor subunit A (IL-17Ra) expression in the fetus to induce MIA-associated phenotypes[11]. We also previously noted that IL-17Ra expression is upregulated in the cortical plate upon MIA. This induction is mostly restricted to ankyrin-3 $(Ank3)^+$ and $NeuN^+$ postmitotic neurons, but not paired box 6 $(Pax6)^+$ neuronal progenitors[20,22,23] (Extended Data Fig. 5a). In line with this observation, knocking out IL-17Ra in offspring using a Cre driver line specific for the nervous system—Nestin-Cre[24]—prevented the development of S1 cortical patches and the associated phenotypes; loss of SATB2 and PV expression or increase in the number of c-Fos^+ neurons was not observed in these animals. As expected, nervous-system-specific abrogation of IL-17Ra in offspring also rescued MIA-induced behavioural abnormalities (Extended Data Fig. 5b–j). Together, these data collectively show that the presence of cortical patches is highly predictive of MIA-induced behaviours. They further suggest that timing of inflammation, composition of maternal gut bacteria, and IL-17Ra expression in the fetal brain dictate the severity of MIA-induced behavioural phenotypes in offspring by contributing to the formation of S1 cortical patches.

Neural activity in S1DZ drives MIA behaviours

Our characterization of cortical patches indicated that an increase in the overall neural activity within S1 could be a major factor driving abnormal behavioural phenotypes in MIA offspring (Fig. 1f, g, Extended Data Fig. 3c–j). Indeed, previous studies suggested that deficits in interneuron development and subsequent perturbations of the excitation/inhibition balance could be the underlying cause(s) of neurodevelopmental disorders[25–34]. We thus asked whether increasing neural activity in S1 could recapitulate MIA-induced behaviours in wild-type adult animals. We virally expressed either enhanced yellow fluorescent protein (EYFP), channelrhodopsin (ChR2)[35] or halorhodopsin (NpHR)[36] using the neuron-specific promoter, human synapsin 1 (hSyn1) (Fig. 3c, Extended Data Fig. 6a). Both the virus and the optical fibres were bilaterally targeted to a region centred on S1DZ (S1DZ region), in which cortical patches were most consistently observed in MIA animals (Fig. 3a). Animals were subsequently subjected to the behavioural assays described above, while receiving optical stimulation at 3-min intervals (a 3 min-'on' session followed by a 3 min-'off' session or vice versa) (Fig. 3b). Increasing neural activity with ChR2 in wild-type offspring resulted in enhanced marble burying behaviours, impaired sociability without any effects on total interaction time, and reduced time spent at the centre of an open field (Fig. 3d–h, Extended Data Fig. 6). On the other hand, photostimulation of EYFP-expressing neurons in the control group failed to induce any MIA-associated behaviour. Furthermore, reducing neural activity in S1 using NpHR did not generate behavioural abnormalities, with the exception of a slight, yet significant, increase in marble burying behaviour compared to the EYFP-expressing control group (Fig. 3e). This effect is probably due to non-specific inhibition of different types of neurons in the photostimulated region. Therefore, to specifically isolate the contribution of only excitatory glutamatergic neurons, we used a Cre-dependent strategy to express opsins under the control of the vesicular glutamate transporter 2 promoter (vGluT2)[37] (Fig. 3i). Increasing activity of $vGluT2^+$ neurons using ChR2 recapitulated all three MIA-associated behaviours, whereas photostimulation in NpHR- or EYFP-expressing animals failed to induce these behavioural abnormalities (Fig. 3j–n, Extended Data Fig. 7a–f). We also selectively modulated neural activity in PV^+ neurons by virally driving Cre-dependent opsin expression in PV-Cre animals[38] (Fig. 3o). Inhibiting the activity of the PV^+ neuronal population with NpHR mimicked the decrease in the number of PV^+ neurons observed in the MIA-cortical patches and recapitulated all three MIA-associated behavioural phenotypes (Fig. 3p–t, Extended Data Fig. 7g–l). On the other hand, photostimulation of EYFP- or ChR2-expressing animals did not produce any observable deficits (Fig. 3q–t).

We next examined whether the ability to drive these MIA behaviours is a general feature of S1 or is specific to the S1DZ region (~AP = −0.5 mm), in which we predominantly observed cortical patches. We targeted ChR2 and optical implants into four additional anterior and posterior regions of S1, while keeping the ML coordinates consistent (Extended Data Fig. 8a–c). Photostimulation of these off-target regions did not elicit MIA phenotypes in the marble burying or sociability assays (Extended Data Fig. 8d–f). The same manipulation carried out

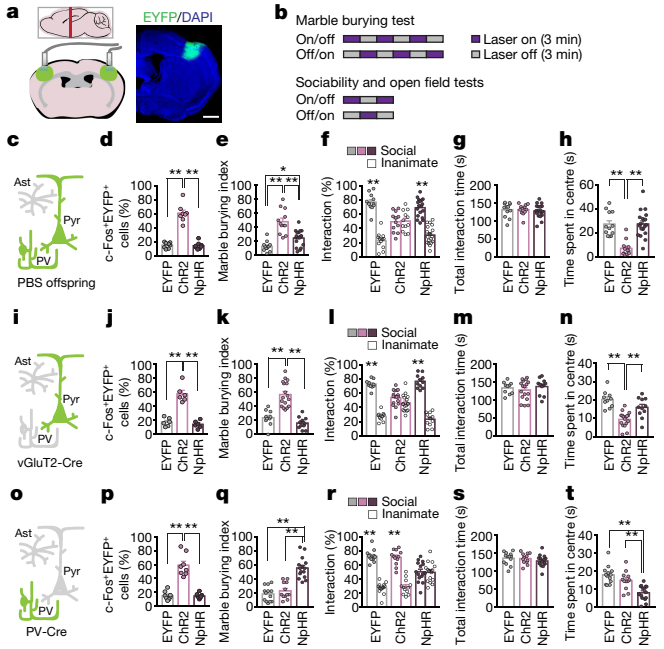

Figure 3 | Increasing neural activity in the S1DZ region induces MIA behavioural phenotypes in wild-type mice. a, Schematics (left) and representative image (right) of EYFP-expressing virus injection site in the S1DZ-centred cortical region. The mouse brain in this figure has been reproduced from ref. 12. Scale bar, 1 mm. **b**, Optical stimulation protocol. Laser was given in a counterbalanced manner. **c**, **i**, **o**, Schematic of labelled cells (green) in PBS offspring (**c**), vGluT2-Cre (**i**), or PV-Cre mice (**o**) (pyr, pyramidal neuron; PV, parvalbumin-positive neuron; ast, astrocyte). **d**, **j**, **p**, Percentage of $EYFP^+$ neurons co-expressing c-Fos upon photostimulation ($n = 8, 8, 8$ mice, 4 independent experiments (PBS offspring; AAV_2-hSyn-EYFP, ChR2, NpHR); $n = 6, 6, 6$ mice, 3 independent experiments (vGluT2-Cre; AAV_2-EF1a-DIO-EYFP, ChR2, NpHR); $n = 8, 8, 8$ mice, 4 independent experiments (PV-Cre; AAV_2-EF1a-DIO-EYFP, ChR2, NpHR)). **e**–**h**, **k**–**n**, **q**–**t**, Marble burying index (18 min) (**e**, **k**, **q**), percentage of interaction (**f**, **l**, **r**) and total interaction time (**g**, **m**, **s**) during the first laser-on session of the sociability test, and time spent in centre during the first laser-on session of the open field test (**h**, **n**, **t**) ($n = 12, 12, 18$ mice, 5 independent experiments (PBS offspring; AAV_2-hSyn-EYFP, ChR2, NpHR); $n = 10, 17, 11$ mice, 5 independent experiments (vGluT2-Cre; AAV_2-EF1a-DIO-EYFP, ChR2, NpHR); $n = 13, 12, 15$ mice, 6 independent experiments (PV-Cre; AAV_2-EF1a-DIO-EYFP, ChR2, NpHR)). $^*P < 0.05$, $^{**}P < 0.01$ calculated by two-way ANOVA (**f**, **l**, **r**) and one-way ANOVA (**d**, **e**, **g**, **h**, **j**, **k**, **m**, **n**, **p**, **q**, **s**, **t**) with Tukey post hoc tests. Graphs indicate mean ± s.e.m.

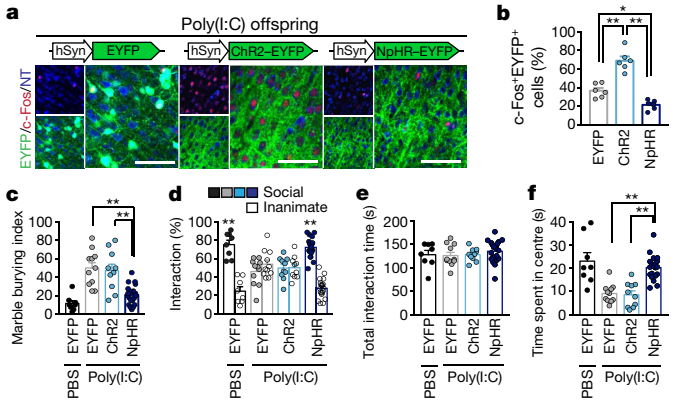

Figure 4 | Reducing neural activity in the S1DZ region corrects behavioural abnormalities in MIA offspring. a, Representative images of c-Fos expression upon photostimulation of the S1DZ region in MIA offspring. Scale bars, 100 μm. **b**, Percentage of EYFP and c-Fos co-expressing neurons upon stimulation ($n = 6, 6, 6$ mice; 3 independent experiments (MIA; AAV_2-hSyn-EYFP, ChR2, NpHR)). **c**–**f**, Performance in the marble burying test (**c**), percentage of interaction (**d**) and total interaction time (**e**) during the sociability test, and time spent in centre during the open field assay (**f**) ($n = 8, 11, 10, 20$ mice; 5, 5, 5, 7 independent experiments (PBS; AAV_2-hSyn-EYFP; MIA; AAV_2-hSyn-EYFP, ChR2, NpHR)). $^*P < 0.05$, $^{**}P < 0.01$ calculated by two-way ANOVA (**d**) and one-way ANOVA (**b**, **c**, **e**, **f**) with Tukey post hoc tests. Graphs indicate mean ± s.e.m.

medially in the forelimb region (S1FL) or laterally in the barrel field of primary somatosensory cortex (S1BF) also failed to induce any behavioural abnormalities (Extended Data Fig. 8g–l). As cortical patches are often observed only in one hemisphere (Extended Data Fig. 1), we asked whether unilateral manipulation of neural activity in the S1DZ region is sufficient to produce MIA behavioural phenotypes. Targeting ChR2 and optical implants to either hemisphere unilaterally increased the number of $c\text{-}Fos^+$ neurons both in ipsilateral as well as contralateral S1 and was capable of driving MIA behaviours similarly to the bilateral stimulation (Extended Data Fig. 9). Taken together, these results demonstrate that MIA behaviours can be recapitulated in wild-type animals either through the activation of excitatory neurons or the inhibition of PV^+ inhibitory neurons and that this feature is primarily localized to the cortical region centred on the S1DZ.

Reducing neural activity rescues MIA behaviours

We next asked whether reduction of neural activity in the S1DZ region of MIA offspring is sufficient to correct the observed behavioural abnormalities. Photostimulation of NpHR-expressing animals decreased the number of $c\text{-}Fos^+$ cortical neurons when compared to those in photostimulated EYFP-expressing MIA animals (Fig. 4a, b, Extended Data Fig. 10a). This inhibition of neural activity was sufficient to suppress enhanced marble burying, restore sociability, and increase the time spent in the centre of the open field to levels observed in control PBS animals (Fig. 4c–f, Extended Data Fig. 10). Photostimulation of EYFP- or ChR2-expressing animals did not rescue any behavioural deficits (Fig. 4c–f). Thus, these data demonstrate that an acute reduction in neural activity in the S1DZ region is sufficient to rescue behavioural abnormalities in MIA offspring prenatally exposed to maternal inflammation.

Subpopulations of S1DZ neurons control MIA behaviours

To gain insight into the downstream neural circuits involved in eliciting MIA-associated behaviours, we next examined the efferent targets of the S1DZ. We injected an anterograde-labelling adeno-associated virus (AAV) driving EYFP into the S1DZ and an AAV driving mCherry into either the S1FL or S1BF. These tracing studies revealed that the S1DZ exhibits largely distinct efferent targets compared to the S1FL and S1BF regions (Fig. 5a, b, Extended Data Fig. 11). The S1DZ selectively sends axons to a sub-region of M2, striatum, and TeA. To test the role of these distinct downstream regions in eliciting MIA-behaviours, we injected retrogradely transported rabies virus[39] expressing EYFP, Chronos (excitatory opsin)[40] or ArchT (inhibitory opsin)[41] into the TeA to label S1DZ neurons in wild-type animals (Fig. 5c, d). Photostimulation of Chronos-positive, TeA-projecting neurons in the S1DZ generated sociability deficits without affecting total interaction time, but failed to induce increased marble burying phenotypes (Fig. 5e–g, Extended Data Fig. 12a–d). Photostimulation of EYFP- or ArchT-expressing neurons did not produce any behavioural deficits. Thus, in otherwise wild-type animals, increasing the neural activity of the neurons in the S1DZ that project to the TeA recapitulated MIA-associated sociability deficits, but not the repetitive marble burying phenotypes. Conversely, in MIA animals, decreasing the neural activity of this S1DZ neuronal population with ArchT restored normal sociability, but failed to suppress the enhanced marble burying phenotype (Fig. 5e–g, Extended Data Fig. 12a–d). We also manipulated the activity of the striatum-projecting S1DZ

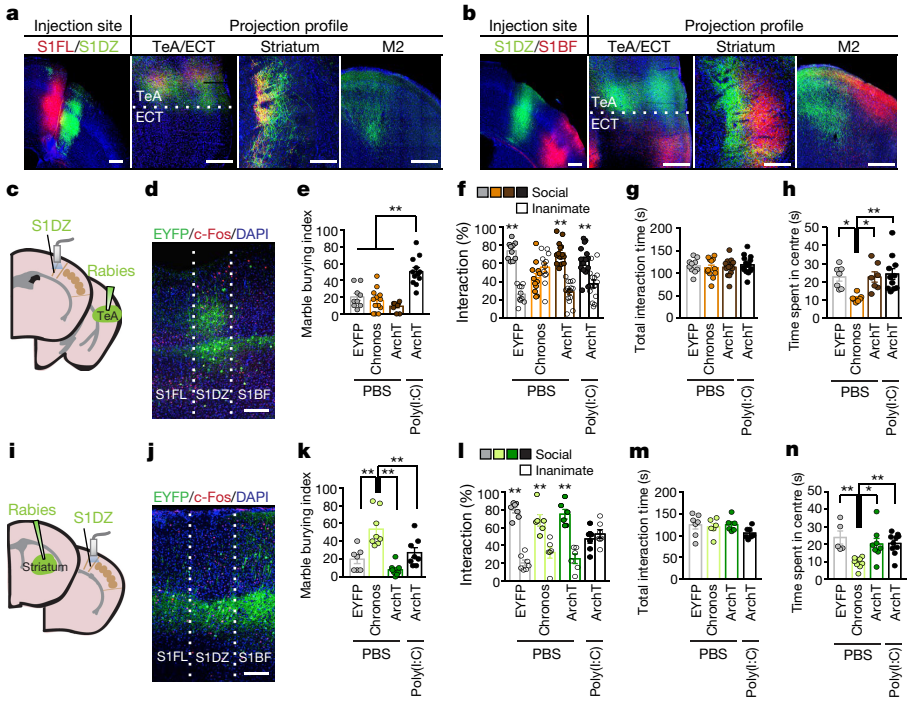

Figure 5 | Distinct populations of S1DZ neurons selectively modulate marble burying and sociability phenotypes. a, **b**, Anterograde-tracing using AAV_2-hSyn-mCherry (S1FL and S1BF) and AAV_2-hSyn-EYFP (S1DZ) ($n = 5$ mice, 4 independent experiments). **c**, **i**, Schematics of optic fibre implantation (S1DZ) and virus injection sites in TeA (**c**) or dorsolateral striatum (**i**). The mouse brain in this figure has been reproduced from ref. 12. **d**, **j**, Representative image of EYFP, c-Fos, and DAPI expression in S1DZ after photostimulation (3 independent experiments). Scale bars, 300 μm. **e**–**h**, **k**–**n**, Performance in the marble burying test (**e**, **k**) (TeA: $n = 9$, 13, 10, 12 mice, 7 independent experiments; striatum: $n = 7$, 8, 8, 8 mice, 5 independent experiments (PBS; RV–EYFP, Chronos, ArchT, MIA; RV-ArchT)), percentage of interaction (**f**, **l**) and total interaction time (**g**, **m**) during the sociability test (TeA: $n = 10$, 12, 15, 15 mice, 7 independent experiments; striatum: $n = 7$, 6, 6, 7 mice, 5 independent experiments (PBS; RV–EYFP, Chronos, ArchT, MIA; RV–ArchT)), and the open field test (**h**, **n**) (TeA: $n = 7$, 7, 7, 11 mice, 7 independent experiments; striatum: $n = 5$, 9, 8, 10 mice; 5 independent experiments (PBS; RV–EYFP, Chronos, ArchT, MIA; RV-ArchT)). $^*P < 0.05$, $^{**}P < 0.01$ calculated by two-way ANOVA (**f**, **l**) and one-way ANOVA (**e**, **g**, **h**, **k**, **m**, **n**) with Tukey post hoc tests. Graphs indicate mean ± s.e.m.

neurons and found that this population, when activated using Chronos, induced enhanced marble burying phenotype in wild-type animals without modulating sociability. Conversely, decreased neural activity in this population suppressed the enhanced marble burying behaviour without correcting sociability deficits in MIA offspring (Fig. 5k–m, Extended Data Fig. 12g–j). The TeA- or striatum-projecting S1DZ populations equally modulated the amount of time spent in the centre of an arena in the open field assay (Fig. 5h, n, Extended Data Fig. 12e, f, k, l). These data suggest that the neurons in S1DZ region projecting to the TeA or striatum selectively modulate interactions with social targets and repetitive behaviours, respectively.

Discussion

Identifying neural circuits and components that modulate behaviours aberrantly manifested in patients with neurodevelopmental disorders is critical for developing therapeutic approaches. One challenge to achieving this goal is the paucity of animal models in which discrete brain areas are known to mediate disorder-associated behavioural symptoms. Here we identified a restricted brain region centred on S1DZ as a component of the neural circuit that mediates MIA-induced behavioural abnormalities. S1DZ has been implicated in proprioceptive functions[13–15]. It will be crucial to elucidate the nature of the afferent information to the S1DZ region and how this information is differentially processed in the downstream targets of healthy and diseased brains. Our data indicate that IL-17Ra expression in the fetal brain is necessary to mediate the MIA effects. The cell type affected by IL-17Ra activation upon MIA, and mechanisms by which the receptor activation induces cortical patches in S1 need to be identified in the future. Furthermore, it is interesting to note that the main efferent targets of the S1DZ, such as the TeA and M2, are also locations in which cortical patches are frequently found in MIA offspring (Fig. 1b, Extended Data Fig. 1b, d). This observation suggests that cortical patch formation in MIA offspring may be intricately linked to concerted neural activity among the connected brain regions. Although similar cortical patches were observed in prefrontal and temporal cortical tissues of children with autism[42], it will be informative to examine whether cortical patches are also found in S1 of human patients with neurodevelopmental disorders. Of note, we cannot rule out a possibility that general MIA-induced behavioural abnormalities are driven by heightened anxiety. It also should be noted that in some MIA animals, cortical patches were only observed outside of S1 (12% of animals, $n = 50$), suggesting that S1DZ region might be one of the nodes within a larger network that controls behaviours affected by MIA. This MIA mouse model with discrete, functionally relevant perturbations in the S1DZ region might provide access to a network that modulates behaviours across different mouse models of neurodevelopmental disorders.

Online Content Methods, along with any additional Extended Data display items and Source Data, are available in the online version of the paper; references unique to these sections appear only in the online paper.

Received 12 December 2016; accepted 16 August 2017.
Published online 13 September 2017.

1. Atladóttir, H. O. *et al.* Maternal infection requiring hospitalization during pregnancy and autism spectrum disorders. *J. Autism Dev. Disord.* **40,** 1423–1430 (2010).
2. Patterson, P. H. Immune involvement in schizophrenia and autism: etiology, pathology and animal models. *Behav. Brain Res.* **204,** 313–321 (2009).
3. Brown, A. S. *et al.* Elevated maternal C-reactive protein and autism in a national birth cohort. *Mol. Psychiatry* **19,** 259–264 (2014).

4. Atladóttir, H. O. *et al.* Association of family history of autoimmune diseases and autism spectrum disorders. *Pediatrics* **124,** 687–694 (2009).
5. Ashwood, P., Wills, S. & Van de Water, J. The immune response in autism: a new frontier for autism research. *J. Leukoc. Biol.* **80,** 1–15 (2006).
6. Lee, B. K. *et al.* Maternal hospitalization with infection during pregnancy and risk of autism spectrum disorders. *Brain Behav. Immun.* **44,** 100–105 (2015).
7. Smith, S. E., Li, J., Garbett, K., Mirnics, K. & Patterson, P. H. Maternal immune activation alters fetal brain development through interleukin-6. *J. Neurosci.* **27,** 10695–10702 (2007).
8. Meyer, U. & Feldon, J. Neural basis of psychosis-related behaviour in the infection model of schizophrenia. *Behav. Brain Res.* **204,** 322–334 (2009).
9. Shi, L., Fatemi, S. H., Sidwell, R. W. & Patterson, P. H. Maternal influenza infection causes marked behavioral and pharmacological changes in the offspring. *J. Neurosci.* **23,** 297–302 (2003).
10. Malkova, N. V., Yu, C. Z., Hsiao, E. Y., Moore, M. J. & Patterson, P. H. Maternal immune activation yields offspring displaying mouse versions of the three core symptoms of autism. *Brain Behav. Immun.* **26,** 607–616 (2012).
11. Choi, G. B. *et al.* The maternal interleukin-17a pathway in mice promotes autism-like phenotypes in offspring. *Science* **351,** 933–939 (2016).
12. Paxinos, G. & Franklin, K. *The Mouse Brain in Stereotaxic Coordinates* 2nd edn (Elsevier Academic Press, 2004).
13. Lee, T. & Kim, U. Descending projections from the dysgranular zone of rat primary somatosensory cortex processing deep somatic input. *J. Comp. Neurol.* **520,** 1021–1046 (2012).
14. Welker, W., Sanderson, K. J. & Shambes, G. M. Patterns of afferent projections to transitional zones in the somatic sensorimotor cerebral cortex of albino rats. *Brain Res.* **292,** 261–267 (1984).
15. Chapin, J. K. & Lin, C. S. Mapping the body representation in the SI cortex of anesthetized and awake rats. *J. Comp. Neurol.* **229,** 199–213 (1984).
16. Gogolla, N. *et al.* Common circuit defect of excitatory–inhibitory balance in mouse models of autism. *J. Neurodev. Disord.* **1,** 172–181 (2009).
17. Orefice, L. L. *et al.* Peripheral mechanosensory neuron dysfunction underlies tactile and behavioral deficits in mouse models of ASDs. *Cell* **166,** 299–313 (2016).
18. Selby, L., Zhang, C. & Sun, Q. Q. Major defects in neocortical GABAergic inhibitory circuits in mice lacking the fragile X mental retardation protein. *Neurosci. Lett.* **412,** 227–232 (2007).
19. Kepecs, A. & Fishell, G. Interneuron cell types are fit to function. *Nature* **505,** 318–326 (2014).
20. Mullen, R. J., Buck, C. R. & Smith, A. M. NeuN, a neuronal specific nuclear protein in vertebrates. *Development* **116,** 201–211 (1992).
21. Kim, S. *et al.* Maternal gut bacteria promote neurodevelopmental abnormalities in mouse offspring. *Nature* http://dx.doi.org/10.1038/23910 (2017).
22. Haubst, N. *et al.* Molecular dissection of Pax6 function: the specific roles of the paired domain and homeodomain in brain development. *Development* **131,** 6131–6140 (2004).
23. Paez-Gonzalez, P. *et al.* Ank3-dependent SVZ niche assembly is required for the continued production of new neurons. *Neuron* **71,** 61–75 (2011).
24. Giusti, S. A. *et al.* Behavioral phenotyping of Nestin-Cre mice: implications for genetic mouse models of psychiatric disorders. *J. Psychiatr. Res.* **55,** 87–95 (2014).
25. Rubenstein, J. L. & Merzenich, M. M. Model of autism: increased ratio of excitation/inhibition in key neural systems. *Genes Brain Behav.* **2,** 255–267 (2003).
26. Chao, H. T. *et al.* Dysfunction in GABA signalling mediates autism-like stereotypies and Rett syndrome phenotypes. *Nature* **468,** 263–269 (2010).
27. Han, S., Tai, C., Jones, C. J., Scheuer, T. & Catterall, W. A. Enhancement of inhibitory neurotransmission by $GABA_A$ receptors having $\alpha_{2,3}$-subunits ameliorates behavioral deficits in a mouse model of autism. *Neuron* **81,** 1282–1289 (2014).
28. Peñagarikano, O. *et al.* Absence of CNTNAP2 leads to epilepsy, neuronal migration abnormalities, and core autism-related deficits. *Cell* **147,** 235–246 (2011).
29. Nelson, S. B. & Valakh, V. Excitatory/inhibitory balance and circuit homeostasis in autism spectrum disorders. *Neuron* **87,** 684–698 (2015).
30. Wöhr, M. *et al.* Lack of parvalbumin in mice leads to behavioral deficits relevant to all human autism core symptoms and related neural morphofunctional abnormalities. *Transl. Psychiatry* **5,** e525 (2015).
31. Canetta, S. *et al.* Maternal immune activation leads to selective functional deficits in offspring parvalbumin interneurons. *Mol. Psychiatry* **21,** 956–968 (2016).
32. Blundell, J. *et al.* Neuroligin-1 deletion results in impaired spatial memory and increased repetitive behavior. *J. Neurosci.* **30,** 2115–2129 (2010).
33. Tabuchi, K. *et al.* A neuroligin-3 mutation implicated in autism increases inhibitory synaptic transmission in mice. *Science* **318,** 71–76 (2007).
34. Etherton, M. R., Blaiss, C. A., Powell, C. M. & Südhof, T. C. Mouse neurexin-1alpha deletion causes correlated electrophysiological and behavioral changes consistent with cognitive impairments. *Proc. Natl Acad. Sci. USA* **106,** 17998–18003 (2009).
35. Zhang, F., Wang, L. P., Boyden, E. S. & Deisseroth, K. Channelrhodopsin-2 and optical control of excitable cells. *Nat. Methods* **3,** 785–792 (2006).
36. Zhang, F. *et al.* Multimodal fast optical interrogation of neural circuitry. *Nature* **446,** 633–639 (2007).
37. Vong, L. *et al.* Leptin action on GABAergic neurons prevents obesity and reduces inhibitory tone to POMC neurons. *Neuron* **71,** 142–154 (2011).
38. Hippenmeyer, S. *et al.* A developmental switch in the response of DRG neurons to ETS transcription factor signaling. *PLoS Biol.* **3,** e159 (2005).
39. Wickersham, I. R., Finke, S., Conzelmann, K. K. & Callaway, E. M. Retrograde neuronal tracing with a deletion-mutant rabies virus. *Nat. Methods* **4,** 47–49 (2007).
40. Klapoetke, N. C. *et al.* Independent optical excitation of distinct neural populations. *Nat. Methods* **11,** 338–346 (2014).
41. Chow, B. Y. *et al.* High-performance genetically targetable optical neural silencing by light-driven proton pumps. *Nature* **463,** 98–102 (2010).
42. Stoner, R. *et al.* Patches of disorganization in the neocortex of children with autism. *N. Engl. J. Med.* **370,** 1209–1219 (2014).

Supplementary Information is available in the online version of the paper.

Acknowledgements We thank J. T. Kwon, M. D. Reed, D. Cho, and S. Bigler for assistance with experiments and B. Noro and C. Jennings for critical reading of the manuscript. This work was supported by the Simons Foundation Autism Research Initiative (J.R.H. and D.R.L.), Simons Foundation to the Simons Center for the Social Brain at MIT (Y.S.Y., J.R.H. and G.B.C.), Robert Buxton (G.B.C.), Hock E. Tan and K. Lisa Yang Center for Autism Research (G.B.C.), the DFG grants CRC/TRR 128 project A07 and WA1600/8-1 (A.W.), the Howard Hughes Medical Institute (D.R.L.), the National Research Foundation of Korea grants MEST-35B-2011-E00012 (S.K.) and NRF-2014R1A1A1006089 (H.K.), the Searle Scholars Program (J.R.H.), the Pew Scholar for Biomedical Sciences (J.R.H.), the Kenneth Rainin Foundation (J.R.H.) and the National Institutes of Health grants R01DK106351 and R01DK110559 (J.R.H.).

Author Contributions Y.S.Y., I.R.W., M.T.H., D.R.L., A.W., J.R.H., and G.B.C. designed the experiments and/or provided advice and technical expertise. Y.S.Y., A.P., J.B., M.L., L.M.P., N.S., J.Y.K., S.K., and H.K. performed the experiments. Y.S.Y., J.R.H., and G.B.C. wrote the manuscript with inputs from the co-authors.

Author Information Reprints and permissions information is available at www.nature.com/reprints. The authors declare no competing financial interests. Readers are welcome to comment on the online version of the paper. Publisher's note: Springer Nature remains neutral with regard to jurisdictional claims in published maps and institutional affiliations. Correspondence and requests for materials should be addressed to J.R.H. (jun_huh@hms.harvard.edu) or G.B.C. (gbchoi@mit.edu).

Reviewer Information *Nature* thanks C. Powell, W. Wetsel and the other anonymous reviewer(s) for their contribution to the peer review of this work.

METHODS

Data reporting. No statistical methods were used to predetermine sample size. The experiments were not randomized. The investigators were blinded to allocation during experiments and outcome assessment for behavioural analyses, voltage-clamp recordings and analysis of cortical patches.

Animals. All experiments were performed in accordance with the Guide for the Care and Use of Laboratory Animals and were approved by the National Institutes of Health and the Committee and Animal Care at Massachusetts Institute of Technology. C57BL/6 mice were purchased from Taconic (USA), and *Nestin-cre* (003771), *PV-cre* (008069), and *vGluT2-cre* (016963) mice from Jackson laboratory (USA). *Il17ra*$^{fl/fl}$ mice were described previously[43]. All mice were crossed and maintained in-house with C57BL/6 mice from Taconic. Mice were analysed with the following primers for the presence of SFB using qPCR: SFB736 forward: 5′-GACGCTGAGGCATGAGAGCAT-3′, SFB844 reverse: 5′-GACGGCACGGATTGTTATTCA-3′ for SFB; UniF340 5′-ACT CCTACGGGAGGCAGCAGT-3′, UniR514 5′-ATTACCGCGGCTGCTGGC-3′ for total commensal bacteria. *Il17ra*$^{fl/fl}$ animals were crossed with *Nestin-cre* to remove IL-17Ra in the brain. The following primers were used to genotype progenies: IL-17Ra-flox-1 forward: 5′-GGCAGCCTTTGGGATCCCAAC-3′, IL-17Ra-flox-2 reverse: 5′- CTACTCTTCTCACCAGCGCGC-3′ for wild-type 336 bp/floxed 377 bp; IL-17Ra-flox-2 reverse, IL-17Ra-flox-3 forward: 5′-GTGCCCACAGAGTGTCTTCTGT-3′ for knockout 478 bp; and Cre forward: 5′-GCGGTCTGGCAGTAAAAACTATC-3′, Cre reverse: 5′-GTGAA ACAGCATTGCTGTCACTT-3′ for Nestin-cre 100 bp. For gender discrimination of each embryo, PCR was carried out using *sry* (sex-determining region of the Y chromosome) gene-specific primers: 5′-ACAAGTTGGCCCAGCAGAAT-3′, and 5′-GGGATATCAACAGGCTGCCA-3′.

Maternal immune activation. Mice were mated overnight and females were checked daily for the presence of seminal plugs, noted as embryonic day 0.5 (E0.5). On E12.5, pregnant female mice were weighed and injected with a single dose of poly(I:C) (20 mg kg^{-1} i.p., Sigma Aldrich), which was incubated at 70 °C for 20 min and cooled down to 25 °C for 1 h before injection. Each dam was returned to its cage and left undisturbed until the birth of its litter. All pups remained with the mother until weaning on postnatal day 21 (P21), at which time mice were group-housed at a maximum of 5 per cage with same-sex littermates. For checking the effect of poly(I:C) administration at different time points during pregnancy, we injected poly(I:C) into pregnant dams on E12.5, E15.5 or E18.5.

Stereotaxic injection. All surgeries were carried out using aseptic techniques and animals were pre-operatively injected with the following dosages of anaesthetics and analgesics: ketamine (100 mg kg^{-1}, i.p.), xylazine (10 mg kg^{-1}, i.p.), and slow-release buprenorphine (1 mg kg^{-1}, s.c.). All stereotaxic reference points were set at Bregma for the AP axis, at the midline for the ML axis, and at the surface of the brain for the DV axis. For optogenetic experiments, animals received bilateral stereotaxic injections of one of the following viruses at rates of $<$0.1 ml min^{-1}: AAV_2-hSyn-EYFP, AAV_2-hSyn-ChR2–EYFP, AAV_2-hSyn-NpHR3.0–EYFP, AAV_2-EF1a-DIO-EYFP, AAV_2-EF1a-DIO-ChR2–EYFP, or AAV_2-EF1a-DIO-NpHR3.0–EYFP (UNC vector core). These viruses were injected into one of the following coordinates: the cortical area near S1DZ (AP = −0.5 mm; ML = ±2.5–3.0 mm; DV = 0.8 mm), off-targets ±0.5 mm or ±1.0 mm along the AP axis (AP = 0.5 mm, ML = ±3.0 mm, DV = 0.8 mm; AP = 0.0 mm, ML = ±3.0 mm, DV = 0.8 mm; AP = −1.0 mm, ML = ±3.0 mm, DV = 0.8 mm; and AP = −1.5 mm, ML = ±3.0 mm, DV = 0.8 mm), S1FL (AP = −0.5 mm, ML = ±2.0 mm, DV = 0.8 mm), or S1BF (AP = −0.5 mm, ML = ±3.5 mm, DV = 0.8 mm). Subsequently, fibre optic implants (300-μm core size, Thorlabs) were bilaterally placed 500-μm above the virus injection sites.

For stimulating the specific S1DZ–TeA and S1DZ–striatum connections, rabies virus (RV–EYFP, RV-Chronos–EYFP or RV-ArchT–EYFP; I.R.W.) was bilaterally introduced into either the TeA (AP = −1.75 mm, ML = ±4.15 mm, DV = 1.65 mm) or striatum (AP = −0.2mm, ML = ±2.7mm, DV = 2.5mm) and optic fibre implants were placed onto the S1DZ (AP = −0.5 mm, ML = ±2.5 mm, DV = 0.3 mm).

For anterograde tracing, AAV_2-hSyn–EYFP was injected into the S1DZ and AAV_2-hSyn–mCherry into either the S1FL or S1BF.

All brain section schematics for showing virus injection sites and optic fibre implantation sites were drawn using Adobe Illustrator to closely resemble the corresponding sections in the Paxinos brain atlas[12].

Behavioural analysis. All behavioural training and testing were carried out in accordance with previously established behavioural schemes[11] with modifications. Animals were tested during light cycle and were transferred to the behaviour testing room with light control (80 Lx) for 1 h before the start of experiments. Experimenters were blind to the treatment group.

Ultrasonic vocalizations. On P9, mouse pup ultrasonic vocalizations (USVs) were detected for 3 min using an Ultra-Sound Gate CM16/CMPA microphone (AviSoft) and SAS Prolab software (AviSoft) in a sound attenuation chamber under stable temperature (19–22 °C). For further characterization of the USVs, the sonograms from the first minute of the recordings were classified into ten distinct categories in accordance with previously established methods[44] and were analysed for the total number of calls made and the average duration of the calls.

Three-chamber social approach assay. Male mice (8–12-week-old) were tested for sociability using a three-chamber social approach paradigm. An empty object-containment cage (circular metallic cages, Stoelting Neuroscience) was each placed into the left and right chambers of a 3-chamber arena (50 cm × 35 cm × 30 cm), which the experimental mice freely investigated for 10 min (exploration period/habituation). The following day, the mice underwent another 10 min exploration period (habituation). Immediately after, the mice were confined to the centre chamber, while a social object (unfamiliar C57BL/6 male mouse) and an inanimate object (rubber object of a similar size as the social object) were placed alternatingly into either the left or right object-containment cage. Barriers to the adjacent chambers were removed, and the mice were allowed to explore the three-chamber arena for 10 min. Approach behaviour was defined as interaction time (that is, sniffing and approach) with targets in each chamber (within 2 cm). Sessions were video-recorded and object approach behaviour and total distance moved were analysed using EthoVision tracking system (Noldus). Percentage of interaction was calculated as the percentage of time spent investigating the social target or the inanimate object out of the total investigation time for both objects.

Marble burying test. Mice were placed into testing arenas (arena size: 40 cm × 20 cm × 30 cm, bedding depth: 3 cm) each containing 20 glass marbles (laid out in four rows of five marbles equidistant from one another). At the end of the 15-min exploration period (18-min period for optogenetics experiments), mice were carefully removed from the testing cages and the number of marbles buried was recorded. The marble burying index was arbitrarily defined as the following: 1 for marbles covered $>$50% with bedding, 0.5 for marbles covered $<$50% with bedding, or 0 for anything less.

Open field test. Mice underwent a 15-min exploration period in the testing arena (arena size: 50 cm × 50 cm × 35 cm). Sessions were video-recorded and analysed for time spent in the centre (centre size: 25 cm × 25 cm) using EthoVision Noldus tracking system (Noldus).

Behavioural analysis with optical stimulation. After two weeks of recovery, animals were assessed using the behavioural schemes described above. During behavioural assays, animals were given 3 min of laser stimulation ('on' session, ChR2: 405 nm, 6 mW, 20 Hz, 50% duty cycle; Chronos: 488 nm, 6 mW, 20 Hz, 50% duty cycle; NpHR3.0 and ArchT: 595 nm, 8 mW, 20 Hz, 50% duty cycle) followed by 3 min of no stimulation ('off' session). Animals started with either an 'on' or 'off' session in a counterbalanced manner. Photostimulation was controlled with a waveform generator (Keysight, 33220A) and EthoVision XT (Noldus). Behavioural analysis was conducted as described earlier using EthoVision Noldus tracking system (Noldus).

For quantitative analysis of photostimulation-dependent activation of virus expressing neurons, mice were killed 1 h after the end of the behavioural testing. Brain slices were double-labelled for c-Fos (sc-7270, Santa Cruz; ABE457, Millipore) and EYFP (ab5450, Abcam). The percentage of neurons expressing c-Fos (c-Fos$^+$EYFP$^+$/EYFP$^+$) within a 500 μm × 500 μm area, 300 μm below the optical fibre placement was calculated. Behavioural results from mice without viral infection or with inaccurate targeting of virus or fibre implantations were excluded. Experimenters were blinded to the treatment groups.

Slice preparation for whole-cell electrophysiology. Mice were anaesthetized with pentobarbital (40 mg kg^{-1}, i.p.) and intracardially perfused with ice-cold dissection buffer (in mM: 87 NaCl, 2.5 KCl, 1.25 NaH_2PO_4, 26 $NaHCO_3$, 75 sucrose, 10 dextrose, 1.3 ascorbic acid, 7 $MgCl_2$ and 0.5 $CaCl_2$) bubbled with 95% O_2 and 5% CO_2. Brains were rapidly removed and immersed in ice-cold dissection buffer. Somatosensory cortical sections were dissected and 300 μm coronal slices were prepared using a Leica VT1200S vibratome (Leica). Slices recovered for 20 min in a 35 °C submersion chamber filled with oxygenated artificial cerebrospinal fluid (aCSF) (in mM: 124 NaCl, 3 KCl, 1.25 NaH_2PO_4, 26 $NaHCO_3$, 1 $MgCl_2$, 2 $CaCl_2$, and 20 glucose) and then kept at room temperature for $>$40 min until use.

Voltage-clamp recordings. To specifically isolate miniature inhibitory postsynaptic currents (mIPSCs), slices were placed in a submersion chamber maintained at 32 °C, perfused at 2 ml min^{-1} with oxygenated aCSF (as described above) containing 1 μM TTX, 100 μM DL-APV, and 20 μM DNQX and held at 0 mV. Cells were visualized using an Olympus BX-51 equipped with infrared differential interference contrast (IR-DIC) optics. Pyramidal neurons from Layer II/III of PBS-control offspring or corresponding upper portion of the cortex of MIA offspring were identified by intrinsic membrane properties present in S1 and morphological confirmation

of spiny dendrites. Patch pipettes were pulled from thick-walled borosilicate glass (P-2000, Sutter Instruments Novato). Open tip resistances were between 2.5–6 MΩ and were back-filled with an internal solution containing the following (in mM): 100 $CsCH_3SO_3$, 15 CsCl, 2.5 $MgCl_2$, 10 HEPES, 5 QX-314, 5 BAPTA, 4 Mg-ATP, 0.3 Mg-GTP, and 0.025 Alexa-568 with pH adjusted to 7.25 with 1 M CsOH and osmolarity adjusted to ~295 mOsm by the addition of sucrose or water. Voltage-clamp recordings were performed in whole-cell configuration using patch-clamp amplifier (Multiclamp 700B, Molecular Devices or Amplifier BVC-700A, Dagan) and data were acquired and analysed using pClamp10 software (Molecular Devices) or a template-matching algorithm in MATLAB. Pipette seal resistances were >1 GΩ and pipette capacitive transients were minimized before breakthrough. Changes in series and input resistance were monitored throughout the experiment by giving a test pulse every 30 s and measuring the amplitude of the capacitive current. Slices were subsequently fixed in 4% PFA for post hoc validation. Cells were discarded if series resistance rose above 20 MΩ. The experimenter was blinded during the acquisition and analysis of the postsynaptic currents.

Immunohistochemistry. For cryosectioning, animals were intracardially perfused, and the brain was dissected out, fixed with 4% PFA in PBS overnight at 4 °C, and cryoprotected in 30% sucrose solution. The left hemisphere was marked with a needle and the sections were coronally sliced at 40 μm using a cryostat (Leica). For vibratome sectioning, animals were intracardially perfused, and the brain was fixed with 4% PFA in PBS overnight at 4 °C. The brains were coronally sliced at either 50 or 100 μm with a Leica VT1000S vibratome (Leica).

Slices were permeabilized with blocking solution containing 0.4% Triton X-100 and 2% goat serum in PBS for 1 h at room temperature and then incubated with anti-rabbit-TBR1 (ab31940, Abcam), anti-mouse-SATB2 (ab51502, Abcam), anti-rabbit-PV (PV27, Swant), anti-rabbit-VIP (20077, Immunostar), anti-mouse-NeuN (MAB377X, Millipore), or anti-rabbit-c-Fos (sc-7270, Santa Cruz; ABE457, Millipore) antibodies overnight at 4 °C. The following day, slices were incubated with fluorescently conjugated secondary antibodies (Invitrogen) for 1 h at room temperature with Neurotrace (Invitrogen) and mounted in Vectashield mounting medium containing 4′,6-diamidino-2-phenylindole, dihydrochloride (DAPI; Vector Laboratories). Images of stained slices were acquired using a confocal microscope (LSM710; Carl Zeiss) with a 20× objective lens; all image settings were kept constant across the same batch of experimental groups.

For anterograde-tracing, brains were sliced into 100-μm sections, and the prepared slices were labelled with anti-chicken-GFP (ab5450, Abcam), anti-rabbit-DsRed (632496, Clontech) and DAPI. Images were acquired with a confocal microscope and then aligned to the Paxinos brain atlas[12].

Double *in situ* hybridization. E14.5 male embryos were obtained from dams treated with poly(I:C) at E12.5. The heads were frozen on dry ice and embedded in Tissue Tek OCT (Sakura Finetek). The blocks were sectioned at 16-μm thickness using a cryostat (Leica). Fluorescent *in situ* hybridization was performed using an amplification technology according to the manufacturer's protocol (ViewRNA ISH Tissue Assay kit, Thermo Fisher Scientific). In brief, the sections were fixed in 4% PFA in PBS at 4 °C for 16–18 h and dehydrated by sequentially soaking the slides in 50%, 70%, and 100% ethanol. *Il17ra* (NM_008359; VB1-10258), *Ank3* (NM_170728; VB6-17256), and *Pax6* (NM_013627; VB6-11573) probes were applied to the sections and incubated for 3 h at 40 °C.

***In situ* hybridization followed by immunohistochemistry.** The sectioned embryo brain slices at 16-μm thickness were fixed in 4% PFA in PBS at room temperature for 10 min and were permeabilized in 70% ethanol at 4 °C for 12–18 h. Sections were further permeabilized in RNase-free 8% SDS for 10 min. Samples were rinsed to remove SDS, and fluorescent *in situ* hybridization for *Il17ra* transcripts were performed according to the manufacturer's protocol (ViewRNA ISH Tissue Assay kit, Thermo Fisher Scientific). The samples were subsequently processed for immunohistochemistry with anti-NeuN antibody (MAB377X, Millipore).

Colocalization coefficients for anterograde-tracing results. Percentage of co-localized projection fibres (co-localization coefficient) from S1FL or S1BF with those from S1DZ was calculated using ImageJ software (Manders' coefficient) (Extended Data Fig. 11). The co-localization coefficient was represented as S1DZ/S1FL or S1FL/S1DZ and S1DZ/S1BF or S1BF/S1DZ. S1DZ/S1FL or S1DZ/S1BF reflects the percentage of S1FL or S1BF projection fibres within the region of interest (ROI) that is co-localized with those from S1DZ. S1FL/S1DZ or S1BF/S1DZ reflects the percentage of S1DZ projection fibres co-localized with those from S1FL or S1BF. Coste's algorithm was used to define the threshold for each image used in this experiment.

Analysis of cortical patches. Cortical patches were identified by the absence of SATB2 or TBR1 expression. Cortical regions that met the following criteria were not included as cortical patches: (1) when the area had weak, but not the absence of, SATB2 or TBR1 expression; (2) when the area displayed tissue damage. Spatial locations of the cortical patches were determined based on their distance from the midline of the brain and the layer structures of the cortex. These locations were matched to their corresponding regions in a mouse brain atlas (Paxinos brain atlas)[12].

For cortical patch analysis of the whole brain (Extended Data Fig. 1), cortical patches were drawn onto a schematic derived from the Paxinos brain atlas[12] using Adobe Illustrator. For closer analysis of those located within AP 0.38 to −1.34 (Extended Data Fig. 2), the brain section schematic was drawn using Adobe Illustrator in reference to the anatomical structures of the coronal section at AP −0.46 in the Paxinos brain atlas[12]. The size of the cortical patches was calculated using Zen Software (Carl Zeiss) and scaled using Adobe Illustrator to reflect the actual size as accurately as possible.

Cell types within the cortical patches of the S1 were characterized by staining brain slices from PBS and MIA offspring for PV, VIP or NeuN in conjunction with SATB2 or TBR1. The cortical region of interest (width: 300 μm), centred on a cortical patch in MIA offspring or the corresponding area in PBS offspring, was divided into 10 equal laminar blocks (bin) representing different depths of the cortex. Individual marker positive cells (SATB2, PV, VIP, or NeuN) were quantified manually. VIP staining was observed both in cells bodies and in processes; only the former was included in counts. Experimenter was blind to the treatment groups.

Conventional RT–PCR. Total RNA was isolated from S1 of adult brains using Quick-RNA mini-prep kits (Zymo). cDNA was synthesized using 200 μg total RNA using oligodT (Protoscript First Strand CDNA Synthesis Kit, NEB). For conventional RT–PCR, 1 μl of cDNA synthesized as described above was diluted in 10 μl of KAPA Taq PCR kit (KAPA Biosystems). *Il17ra* and *Gapdh* mRNA expression were assessed using the following primers: *Il17ra* 5′-CCACTCTGTAGCACCCCAAT-3′ and 5′-CAGGCTCCGTAGTTCCTCAG-3′; *Gapdh* 5′-GACTTCAACAGCCTCCCACTCTTCC-3′ and 5′-TGGGTGGT CCAGGTTTCTTACTCCTT-3′.

Statistics and reproducibility. Statistical analyses were performed using Prism software. The results from behavioural experiments and quantification of individual marker-positive cells were tested using one-way, two-way, or two-way repeated measures ANOVAs followed by Tukey post hoc tests or unpaired two-tailed *t*-test. The correlation between behavioural severity and cortical patch size was tested using linear regression. The distribution of cortical patches was tested using Kruskal–Wallis test followed by Dunn post hoc test. Sample sizes were chosen with adequate power based on the literature as well as our previous studies, in general without using statistical methods to predetermine sample size[11]. Animals were randomized into different groups with approximately comparable numbers of animals in each group whenever possible. No samples or data points were arbitrarily excluded from statistical analysis. Key experiments, including the location of cortical patches, anterograde tracing experiments, and behavioural experiments with optical modulation, were all independently repeated with similar observations. All data are represented as mean ± s.e.m.

Data availability. Source Data containing raw data for the main and Extended Data figures are available in the online version of the paper. All other data are available from the corresponding authors upon reasonable request.

43. El Malki, K. *et al.* An alternative pathway of imiquimod-induced psoriasis-like skin inflammation in the absence of interleukin-17 receptor a signaling. *J. Invest. Dermatol.* **133,** 441–451 (2013).
44. Scattoni, M. L., Gandhy, S. U., Ricceri, L. & Crawley, J. N. Unusual repertoire of vocalizations in the BTBR T+tf/J mouse model of autism. *PLoS One* **3,** e3067 (2008).

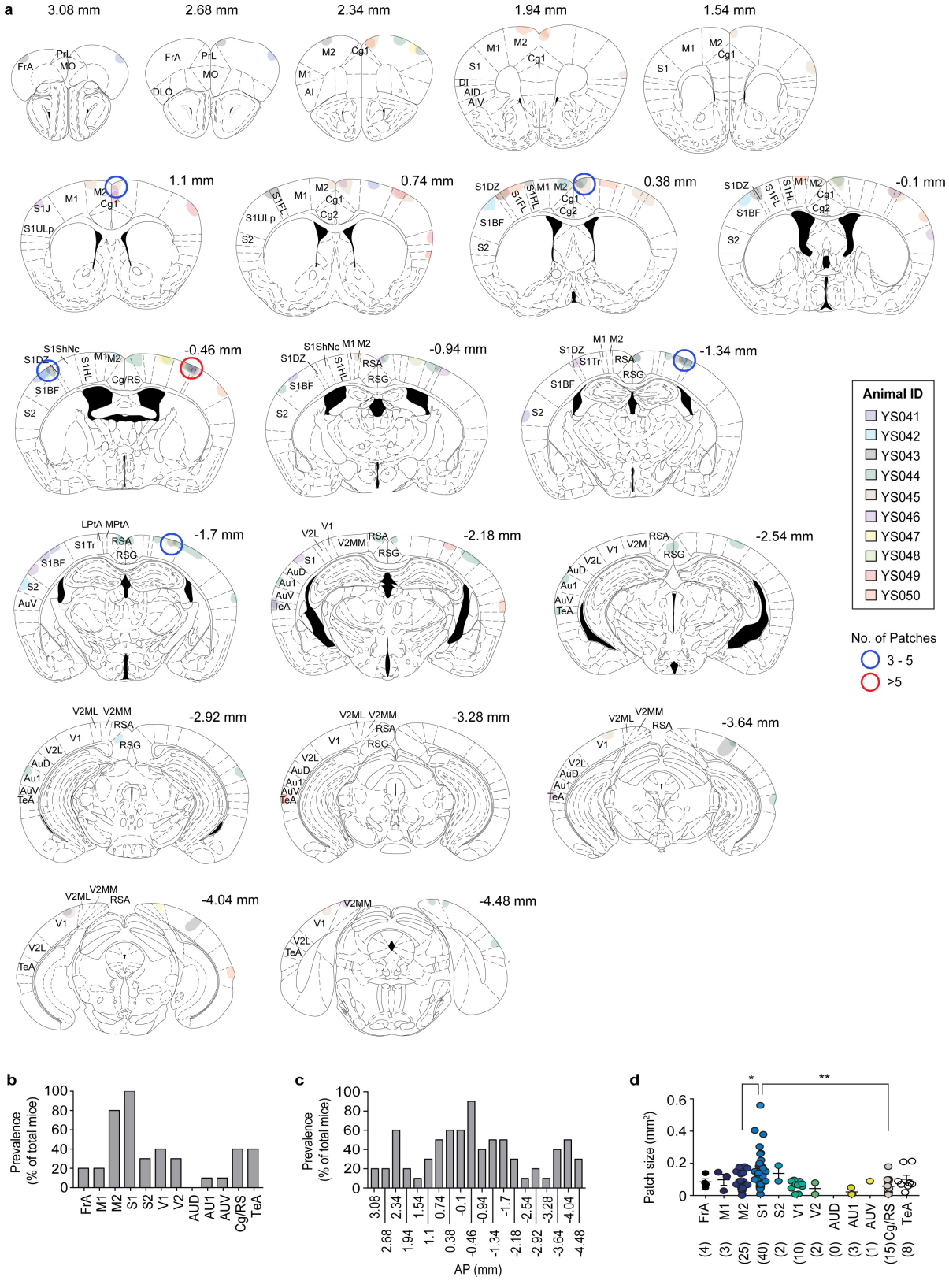

Extended Data Figure 1 | See next page for caption.

Extended Data Figure 1 | Distribution of cortical patches in the cortex of MIA offspring. a, The locations of the cortical patches of 10 individual MIA animals were matched to their corresponding AP levels in ref. 12. Different colours represent the patches from different mice. The sub-regions, in which the cortical patches were observed in more than 3 or 5 animals, are circled in blue or red, respectively. The mouse brain in this figure has been reproduced from ref. 12. **b**, Prevalence of cortical patches in different cortical sub-regions of the MIA offspring described in **a** ($n = 10$ mice, 2 independent experiments). **c**, Prevalence of cortical patches at different AP levels of the brain in the MIA offspring described in **a** ($n = 10$ mice, 2 independent experiments). Individual AP levels correspond to those in the schematic images of **a**. **d**, The size and frequencies of cortical patches found in different cortical sub-regions of the MIA offspring described in **a** ($n = 10$ mice, 2 independent experiments). PrL, prelimbic; MO, medial orbital; DLO, dorsolateral orbital; DI, dysgranular insular; FrA, frontal association cortex; M1, primary motor cortex; M2, secondary motor cortex; S1, primary somatosensory cortex; S2, secondary somatosensory cortex; V1, primary visual cortex; V2, secondary visual cortex; AUD, secondary auditory cortex, dorsal area; AU1, primary auditory cortex; AUV, secondary auditory cortex, ventral area; Cg/RS, cingulate/retrosplenial cortex; TeA, temporal association cortex. $^{*}P < 0.05$, $^{**}P < 0.01$ calculated by Kruskal–Wallis one-way ANOVA with Dunn post hoc test (**d**). Graphs indicate mean ± s.e.m.

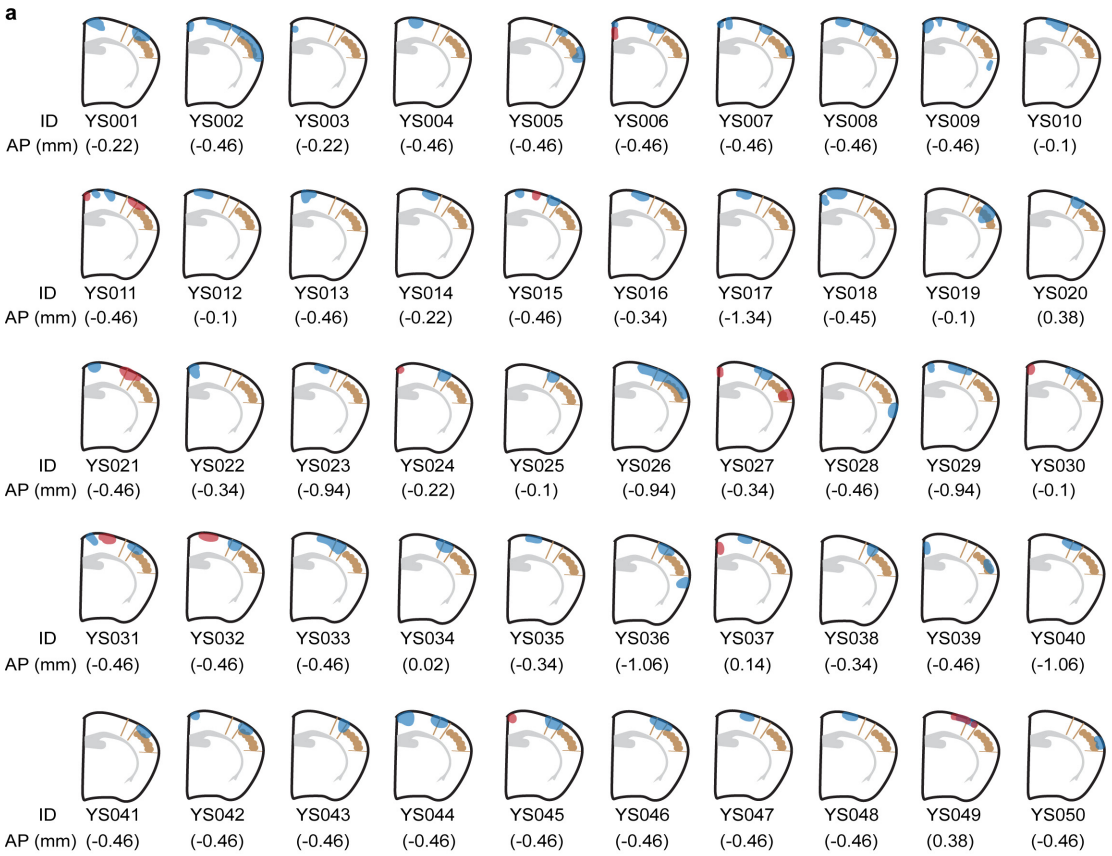

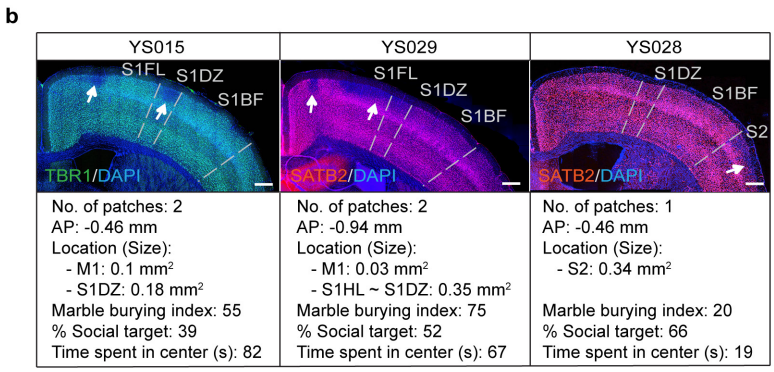

Extended Data Figure 2 | Distribution of cortical patches located within 0.38 to −1.34 mm AP in the brains of MIA offspring. a, Schematics of the cortical patches located within 0.38 to −1.34 mm AP in the brains of MIA offspring plotted onto the atlas plane near −0.46 mm AP. The size of the cortical patches in the schematic is scaled to reflect the actual size as accurately as possible. Blue indicates the cortical patches from one hemisphere and red from the other. The mouse brain in this figure has been reproduced from ref. 12. **b**, Representative images of the cortical patches in the brains of MIA offspring (**a**) stained with TBR1 or SATB2 and counterstained with DAPI. The number, locations, and sizes of the cortical patches observed at a given AP level along with each animal's behavioural performance in the marble burying (marble burying index), sociability (% social target), and the time spent in the centre (s) of an open field are indicated. White arrows indicate cortical patches. Scale bars, 300 μm.

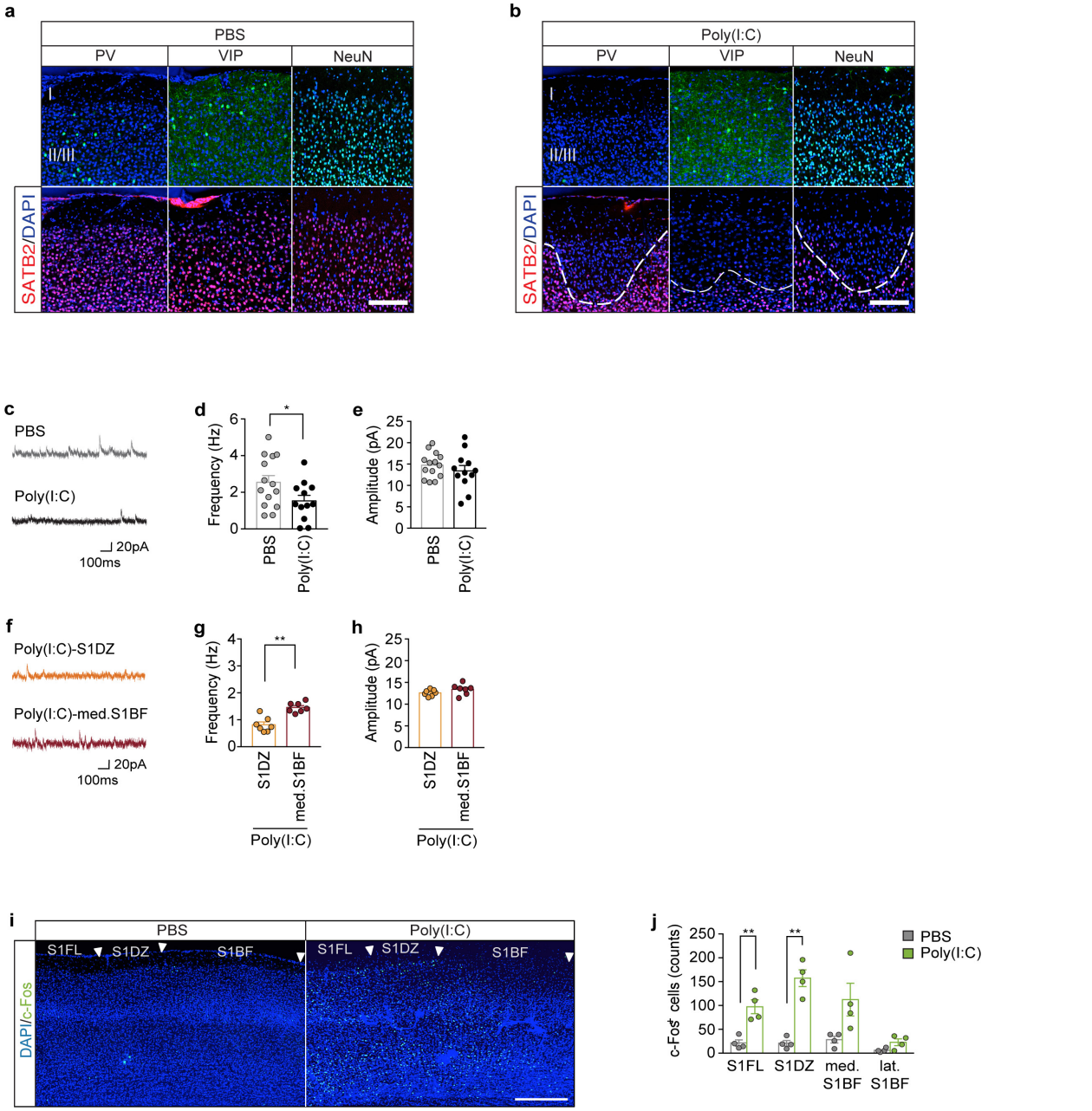

Extended Data Figure 3 | MIA offspring display reduced inhibitory drive onto pyramidal neurons in S1 cortical patches. a, Images cropped in layer I, II, and III of S1 and stained for SATB2 (red) and PV, VIP, or NeuN (green) in offspring from PBS (**a**) or poly(I:C) (**b**) injected dams. Brain slices are counterstained with DAPI (blue). White dotted lines indicate the boundary of cortical patches in MIA offspring. Scale bars, 100 μm. For images shown in Fig. 1d. **c**. Representative traces of mIPSCs from pyramidal neurons in S1DZ of PBS or MIA offspring. **d**, **e**, Average population data depicting the frequency (**d**) and amplitude (**e**) of pharmacologically isolated mIPSCs from S1DZ pyramidal neurons described in **c** ($n = 14$ biological independent samples, 6 mice, 6 independent experiments and 12 biological independent samples, 6 mice, 6 independent experiments from PBS and MIA offspring, respectively). **f**, Representative traces of mIPSCs from pyramidal neurons in S1DZ or medial (med.) S1BF of MIA offspring. **g**, **h**, Average population data depicting the frequency (**g**) and amplitude (**h**) of pharmacologically isolated mIPSCs from S1 pyramidal neurons described in **f** ($n = 7$ biological independent samples, 3 mice, 3 independent experiments and 7 biological independent samples, 3 mice, 3 independent experiments for S1DZ and medial S1BF from MIA offspring, respectively). **i**, Representative image of the S1, stained with DAPI (blue) and for c-Fos (green) from adult offspring of PBS- or poly(I:C)-treated mother. Arrowheads indicate the boundaries of different subregions in the S1. Scale bar, 300 μm. S1FL, primary somatosensory, forelimb; S1DZ, primary somatosensory, dysgranular zone; S1BF, primary somatosensory, barrel field. **j**, Quantification of c-Fos$^+$ cells throughout the S1 ($n = 4$ PBS and 4 poly(I:C) mice, 4 independent experiments). $^*P < 0.05$, $^{**}P < 0.01$ calculated by two-tailed unpaired *t*-test (**d**, **e**, **g**, **h**, **j**). Graphs indicate mean ± s.e.m.

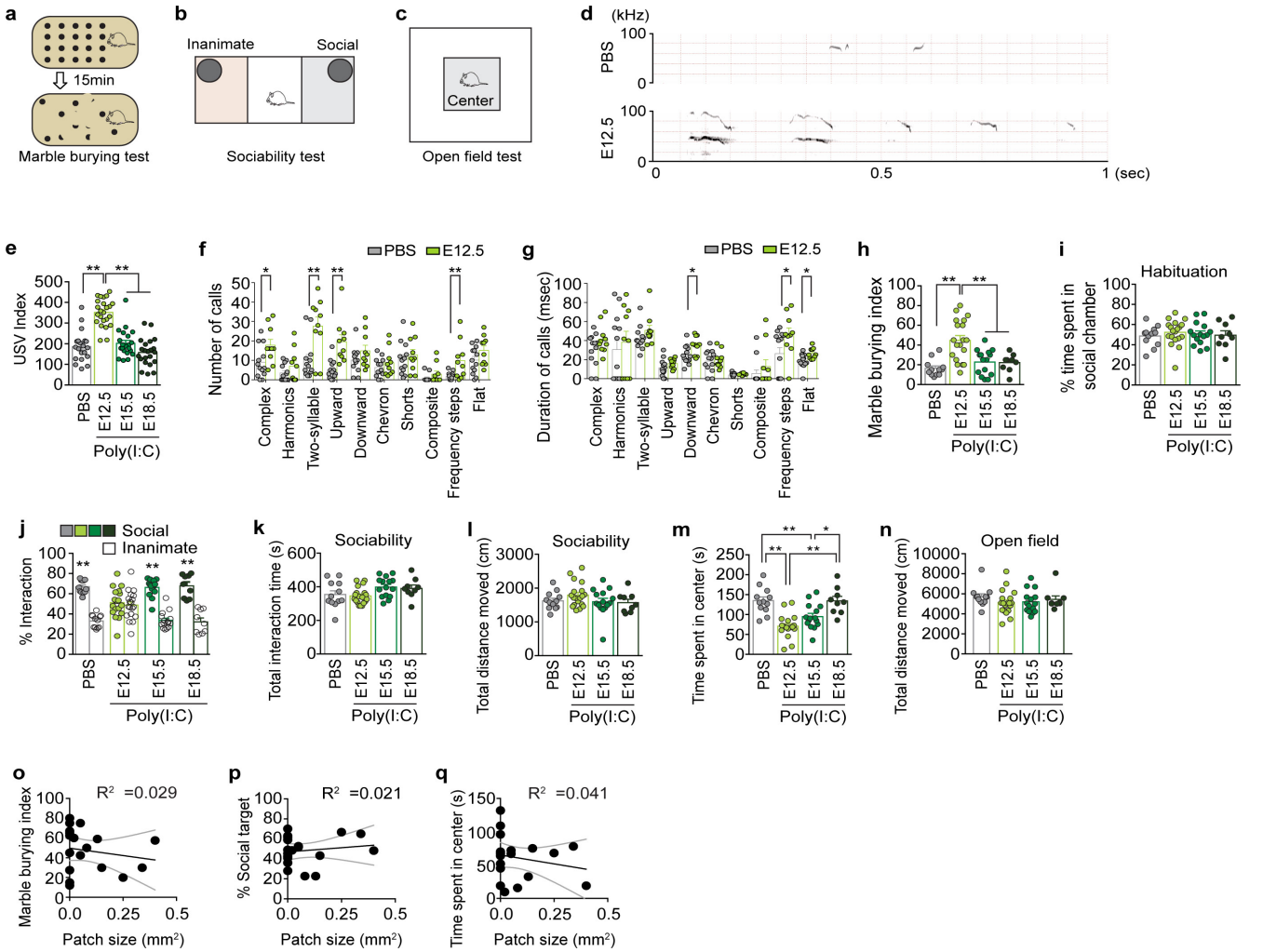

Extended Data Figure 4 | The development of MIA-associated behaviours depends on the time point at which MIA is induced. **a**–**c**, Schematics of the marble burying test (**a**), sociability test (**b**), and open field test (**c**). **d**, Representative spectrographs of the ultrasonic vocalization (USV) for PBS and E12.5. **e**, The USV index represents the number of USVs made by the pups ($n = 20$, 24, 21, and 22 mice for PBS, E12.5, E15.5, and E18.5 groups, 5 independent experiments). **f**, **g**, The sonograms of USVs emitted by the pups are classified into ten distinct categories and analysed for the number of calls made and the duration of the calls (ms) within the first minute of the recording ($n = 13$ and 10 for pups from PBS- and poly(I:C)-injected mothers, respectively, at E12.5, 3 independent experiments). **h**–**n**, The marble burying index (the percentage of marbles buried during the 15-min marble burying test) (**h**), percentage of time spent in the social chamber during habituation period of the sociability test (**i**), percentage interaction during the sociability test (the percentage of time spent investigating the social or inanimate stimulus out of the total exploration time of both objects during the 10-min sociability test) (**j**), the total interaction time (the total exploration time of both objects during the 10-min sociability test) (**k**), the total distance moved during the sociability test (**l**), the time spent in the centre of an open field (**m**), and the total distance moved during the open field test (**n**) of the adult offspring described in **e** ($n = 12$, 19, 15, 9 mice; 7, 7, 7, 5 independent experiments for PBS, E12.5, E15.5, E18.5 groups). **o**–**q**, The size of cortical patches found outside of S1 (within AP 0.38 to −1.34 mm) in offspring from dams injected with poly(I:C) at E12.5 is plotted against the severity of the featured MIA phenotypes on the marble burying test (**o**), sociability test as the percentage of social target (the percentage of time spent investigating the social stimulus out of the total exploration time of both objects) (**p**), and open field test (**q**). Black solid lines represent the regression line and grey lines represent 95% confidence intervals ($n = 19$ mice, 7 independent experiments) for E12.5 group. $^*P < 0.05$, $^{**}P < 0.01$ calculated by two-tailed unpaired *t*-test (**f**, **g**), two-way ANOVA with Tukey post hoc tests (**j**), one-way ANOVA with Tukey post hoc tests (**e**, **h**, **i**, **k**, **l**, **m**, **n**), and linear regression (**o**, **p**, **q**). Graphs indicate mean ± s.e.m.

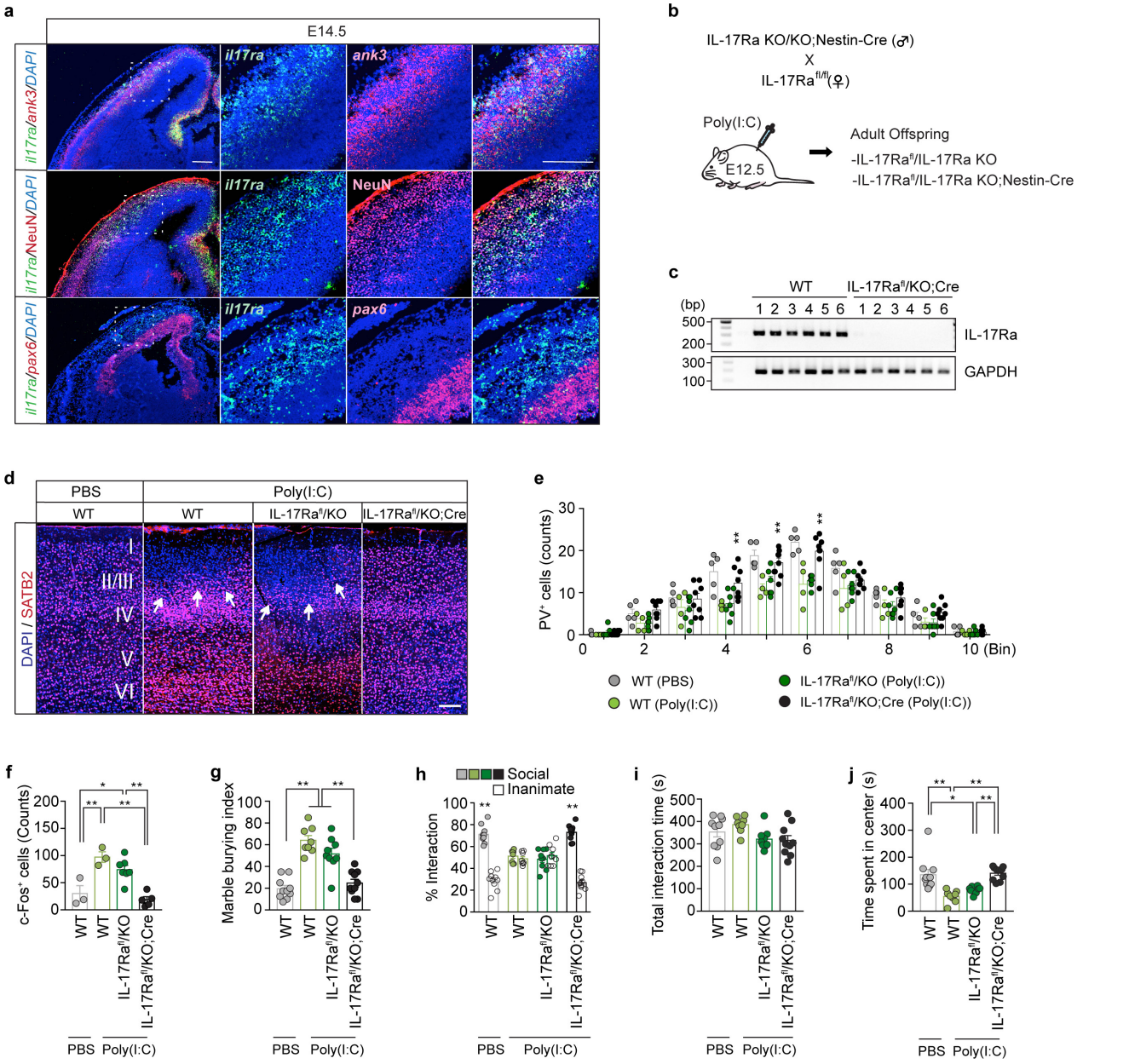

Extended Data Figure 5 | IL-17Ra expression is required in the fetal brain to induce behavioural abnormalities upon MIA. a, Representative images of the embryonic cortex at E14.5 stained for *Il17ra* (green) and *Ank3*, NeuN or *Pax6* (red) in offspring from poly(I:C)-injected dams. Brain slices were counterstained with DAPI (blue) ($n = 3$ mice, 2 independent experiments). Scale bars, 200 μm. **b**, Schematic showing the breeding scheme. Homozygous IL-17Ra-KO animals carrying Nestin-Cre transgene were crossed to homozygous IL-17Ra conditional line (*Il17ra*$^{fl/fl}$). **c**, *Il17ra* and *Gapdh* mRNA expression levels in S1 of wild-type or IL-17Ra$^{fl/KO}$-Cre mice were measured using conventional RT–PCR. Image indicates mRNA expression levels found in individual animals ($n = 6$ mice, 2 independent experiments). **d**, Representative images of SATB2 (red) expression in S1 of offspring with indicated genotypes (wild-type, IL-17Ra$^{fl/KO}$, or IL-17Ra$^{fl/KO}$-Cre) from mothers injected with PBS or poly(I:C) ($n = 5$, 4, 7, and 8 mice from wild-type (PBS), wild-type (poly(I:C)), IL-17Ra$^{fl/KO}$ (poly(I:C)), and IL-17Ra$^{fl/KO}$-Cre (poly(I:C)), 4 independent experiments). Scale bar, 100 μm. **e**, Quantification of PV-positive cells in regions centred on S1 cortical patches around AP −0.46 mm, divided into ten equal bins representing different depths of the cortex, of MIA offspring or in corresponding regions of PBS offspring with indicated genotypes ($n = 5$, 4, 7, and 8 mice from wild-type (PBS), wild-type (poly(I:C)), IL-17Ra$^{fl/KO}$ (poly(I:C)), and IL-17Ra$^{fl/KO}$-Cre (poly(I:C)), 4 independent experiments). **f**, Quantification of c-Fos^{+} cells in the S1 at around AP −0.46 mm ($n = 3$, 3, 7, and 5 mice, from wild-type (PBS), wild-type (poly(I:C)), IL-17Ra$^{fl/KO}$ (poly(I:C)), and IL-17Ra$^{fl/KO}$-Cre (poly(I:C)), 4 independent experiments). **g**–**j**, The marble burying index (**g**), the percentage of interaction (**h**) and the total interaction time (**i**) during the sociability test, and the time spent in the centre of an open field (**j**) of the adult offspring described in **b** ($n = 10$, 8, 9, and 10 mice for wild-type (PBS), wild-type (poly(I:C)), IL-17Ra$^{fl/KO}$ (poly(I:C)), and IL-17Ra$^{fl/KO}$-Cre (poly(I:C)) groups, 5 independent experiments). $^{*}P < 0.05$, $^{**}P < 0.01$ calculated by two-way repeated measures ANOVA with Tukey post hoc tests for statistical comparison between the wild-type (poly(I:C)) and IL-17Ra$^{fl/KO}$-Cre (poly(I:C)) (**e**), one-way ANOVA with Tukey post hoc tests (**f**, **g**, **i**, **j**), and two-way ANOVA with Tukey post hoc tests (**h**). Graphs indicate mean ± s.e.m.

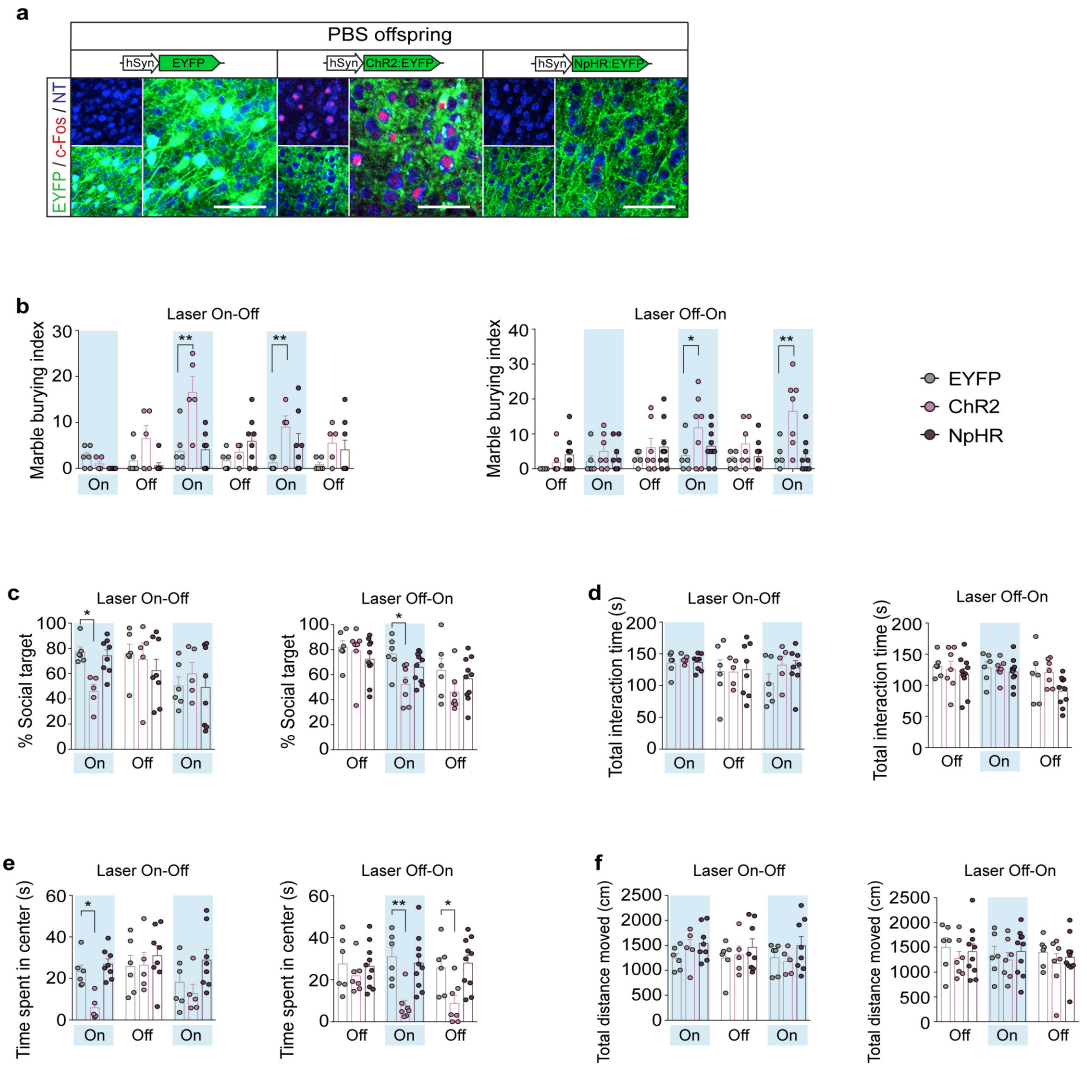

Extended Data Figure 6 | Increasing neural activity in wild-type animals induces MIA behavioural phenotypes. a, Representative images of c-Fos expression upon photostimulation of the S1DZ in wild-type offspring from mothers injected with PBS at E12.5 (PBS offspring). In these animals, AAV_2-hSyn-EYFP, ChR2–EYFP, or NpHR–EYFP viruses were targeted to the S1DZ. Coronal sections of the brains were stained for c-Fos (red) and EYFP (green), and counterstained with neurotrace (NT, blue). Scale bars, 100 μm. **b**–**f**, The marble burying index (the percentage of marbles buried during the 18-min marble burying test) (**b**), the percentage of social target (the percentage of time spent investigating the social stimulus out of the total exploration time of both objects) (**c**), the total interaction time during the sociability test (**d**), the time spent in the centre of an open field (**e**), and the total distance moved during the open field test (**f**) are plotted as averages from each individual 3-min session. Light blue indicates the laser 'On' sessions ('Laser On-Off': $n = 6$, 5, and 8 mice, 4 independent experiments; 'Laser Off-On': $n = 6$, 7, and 10 mice, 4 independent experiments from the AAV_2-hSyn-EYFP, ChR2–EYFP, or NpHR–EYFP injected PBS offspring). $^*P < 0.05$, $^{**}P < 0.01$ calculated by two-way repeated measures ANOVA with Tukey post hoc tests. Graphs indicate mean ± s.e.m.

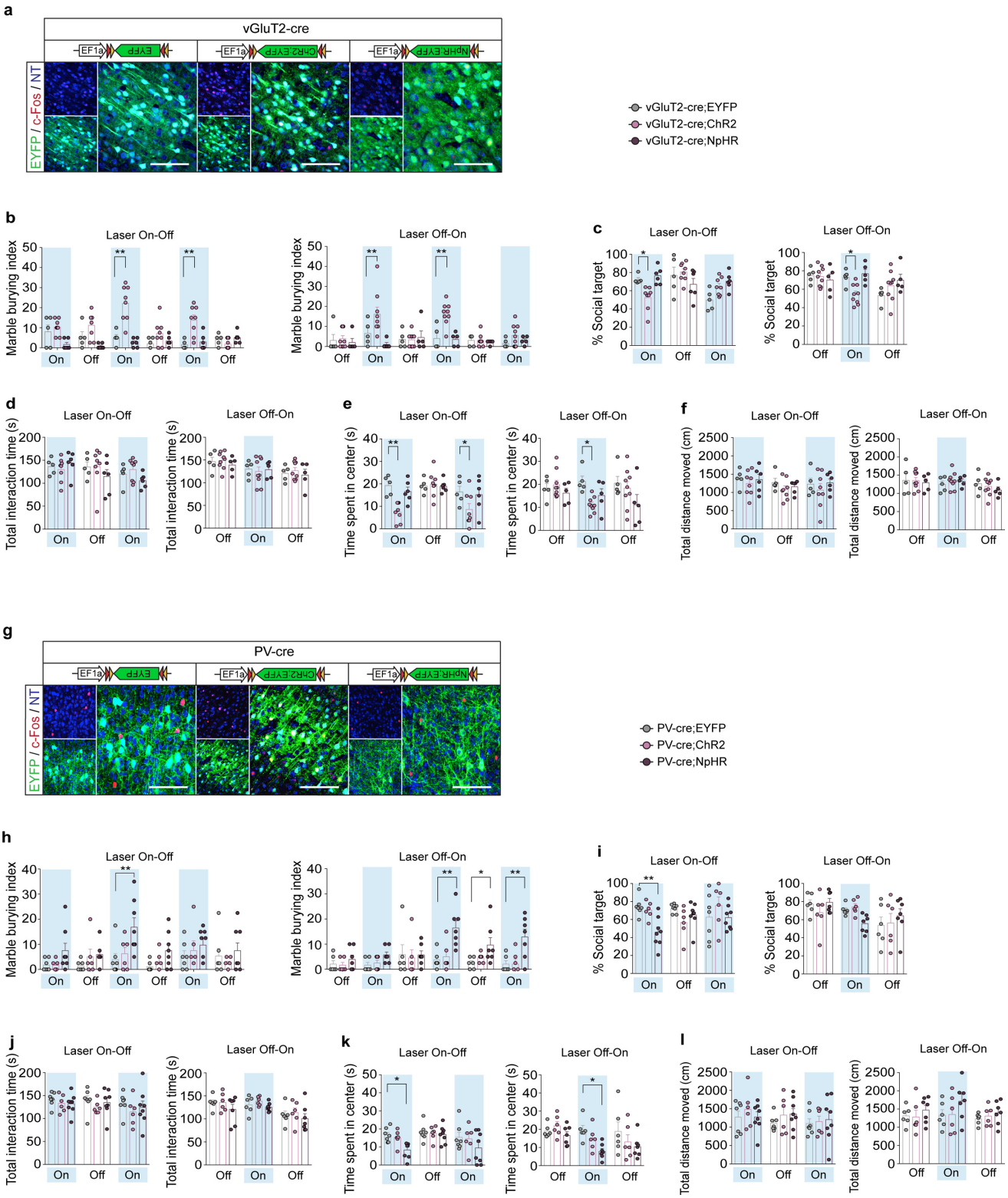

Extended Data Figure 7 | Increasing neural activity in vGluT2-positive neurons or decreasing neural activity in PV-positive neurons of wild-type animals creates MIA behavioural phenotypes. a, **g**, Representative images of c-Fos expression upon photostimulation of the S1DZ in vGluT2-Cre (**a**) or PV-Cre (**g**) animals injected with AAV_2-EF1α-DIO-EYFP, ChR2–EYFP, or NpHR–EYFP viruses. Coronal sections of the brains were stained for c-Fos (red) and EYFP (green), and counterstained with neurotrace (NT, blue). Scale bars, 100 μm. **b**–**l**, The marble burying index, the percentage of social target, the total interaction time during the sociability test, the time spent in the centre of an open field, and the total distance moved during the open field test with vGluT2-Cre (**b**–**f**) and PV-Cre (**h**–**l**) animals are plotted as averages from each individual 3-min session. Light blue indicates the laser 'On' sessions ('Laser On-Off': $n = 5$, 8, and 6 mice, 4 independent experiments; 'Laser Off-On': $n = 5$, 9, and 5 mice, 5 independent experiments for vGluT2-Cre animals injected with AAV_2-EF1α-DIO-EYFP, ChR2–EYFP, and NpHR–EYFP; 'Laser On-Off': $n = 7$, 6, and 8 mice, 6 independent experiments; 'Laser Off-On': $n = 6$, 6, and 7 mice, 5 independent experiments for PV-Cre animals injected with AAV_2-EF1α-DIO-EYFP, ChR2–EYFP, and NpHR–EYFP). $^*P < 0.05$, $^{**}P < 0.01$ calculated by two-way repeated measures ANOVA with Tukey post hoc tests. Graphs indicate mean ± s.e.m.

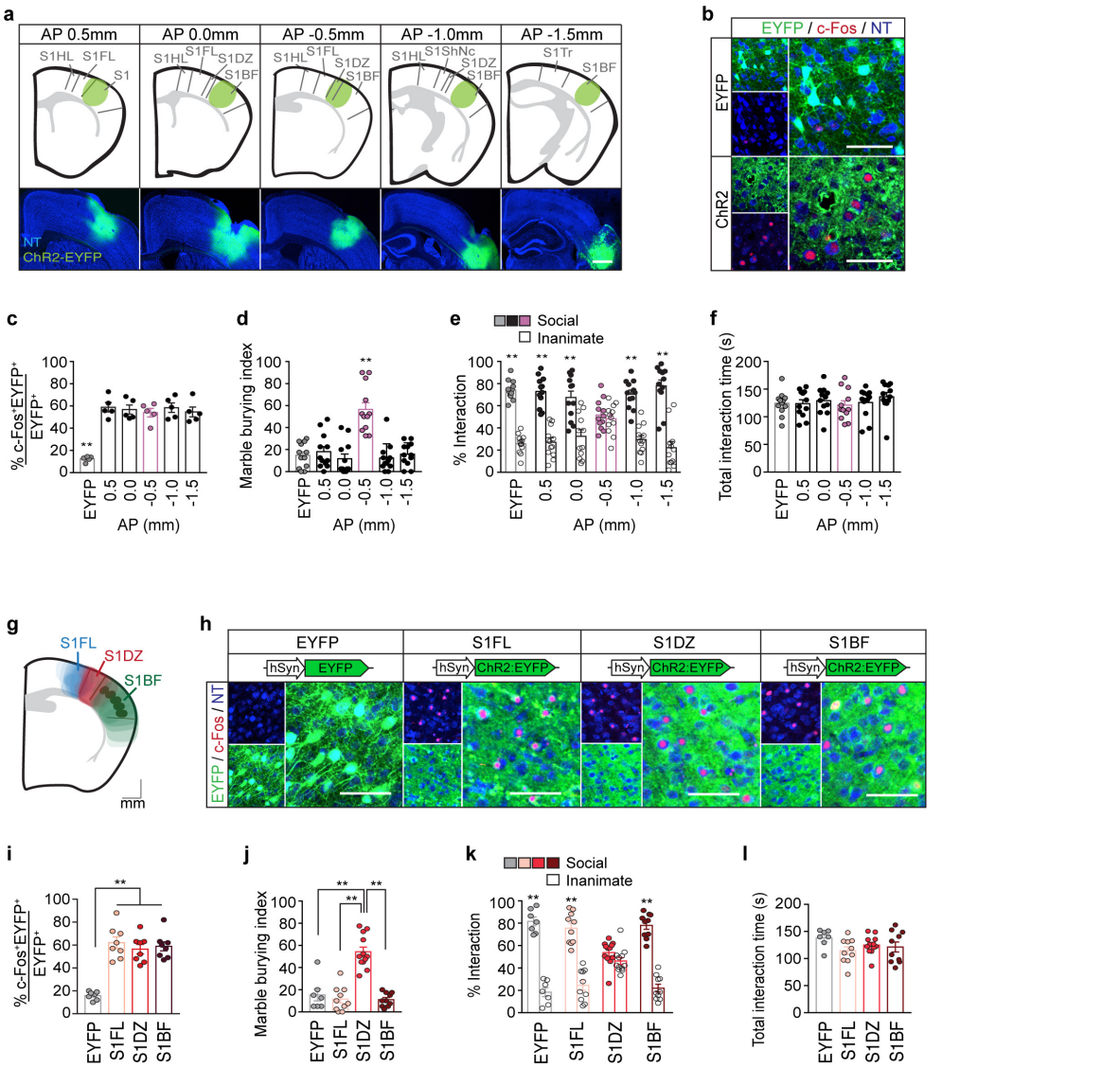

Extended Data Figure 8 | The ability to create MIA behavioural phenotypes by increasing neural activity in wild-type animals is specific with respect to the AP level and the sub-region of the primary somatosensory cortex. a, Schematics (top) and representative images (bottom) of the five sites in the S1 of wild-type animals injected with either AAV_2-hSyn-EYFP or AAV_2-hSyn-ChR2–EYFP virus (green) (AP = +0.5, +0.0, −0.5, −1.0, or −1.5 mm). The mouse brain in this figure has been reproduced from ref. 12. Scale bar, 300 μm. **b**, Representative images of c-Fos expression upon photostimulation of the injection sites in animals as prepared in **a**. Coronal sections of the brains were stained for c-Fos (red) and EYFP (green), and counterstained with neurotrace (NT, blue). Scale bars, 100 μm. **c**, The percentage of $EYFP^+$ neurons expressing c-Fos upon photostimulation of the injection site ($n = 5$ for wild-type animals injected with AAV_2-hSyn-EYFP at AP = −0.5mm and $n = 5, 5, 5, 5$, and 5 for animals injected with AAV_2-hSyn-ChR2–EYFP at AP = 0.5, 0.0, −0.5, −1.0, and −1.5 mm, 3 independent experiments, respectively). **d**–**f**, The marble burying index (**d**), the percentage of interaction (during the first laser-on session) of the sociability test (**e**), and the total interaction time (during the first laser-on session) of the sociability test (**f**) for animals prepared as in (**a**) ($n = 12$ for wild-type animals injected with AAV_2-hSyn-EYFP at AP = −0.5mm and $n = 12, 12, 12, 12$, and 12 for those injected with AAV_2-hSyn-ChR2–EYFP at AP = 0.5, 0.0, −0.5, −1.0, or −1.5 mm, respectively, 6 independent experiments). **g**, A schematic showing the superimposed virus injection sites from individual wild-type animals, in which AAV_2-hSyn-ChR2–EYFP was delivered into the S1FL (blue), S1DZ (red), or S1BF (green). The mouse brain in this figure has been reproduced from ref. 12. **h**, Representative images of c-Fos expression upon photostimulation of the injection sites shown in **g**. Coronal sections of the brains were stained for c-Fos (red) and EYFP (green), and counterstained with neurotrace (NT, blue). Scale bars, 100 μm. **i**, The percentage of $EYFP^+$ neurons co-expressing c-Fos upon photostimulation of the injection site ($n = 7$ mice for EYFP and 8 mice for S1FL, S1DZ, and S1BF; 3 independent experiments). **j**–**l**, The marble burying index (**j**), the percentage interaction (during the first laser-on session) of the sociability test (**k**), and the total interaction time (during the first laser-on session) of the sociability test (**l**) for animals prepared as in **g** ($n = 7$ for wild-type animals injected with AAV_2-hSyn-EYFP into S1DZ and $n = 10$, 12, and 10 for wild-type animals injected with AAV_2-hSyn-ChR2–EYFP into S1FL, S1DZ, and S1BF; 3 independent experiments). S1HL, primary somatosensory, hindlimb; S1FL, primary somatosensory, forelimb; S1, primary somatosensory cortex; S1DZ, primary somatosensory, dysgranular zone; S1BF, primary somatosensory, barrel field; S1ShNc, primary somatosensory, shoulder and neck; S1Tr, primary somatosensory, trunk. $^*P < 0.05$, $^{**}P < 0.01$ calculated by two-way ANOVA with Tukey post hoc tests (**e**, **k**) and one-way ANOVA with Tukey post hoc tests (**c**, **d**, **f**, **i**, **j**, **l**). Graphs indicate mean ± s.e.m.

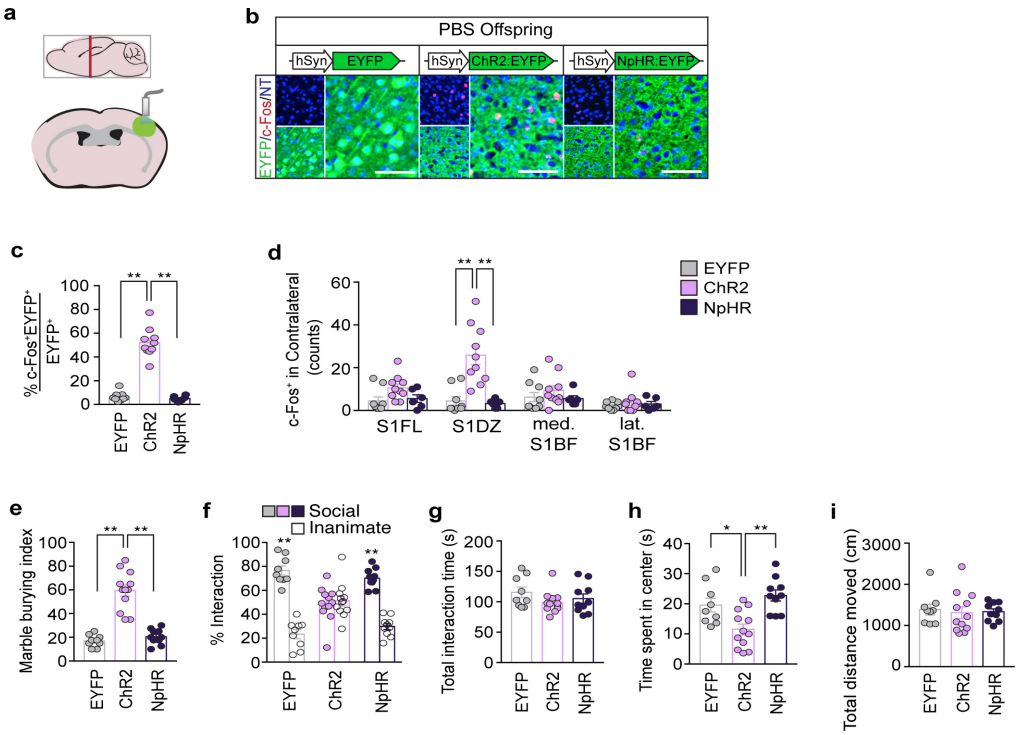

Extended Data Figure 9 | Unilateral increase in neural activity of the S1DZ region creates MIA behaviours in wild-type animals. a, Schematic showing the unilateral virus injection and optic-fibre implantation in the S1DZ of wild-type animals injected with AAV_2-hSyn-EFYP, ChR2–EYFP, or NpHR–EFYP. The mouse brain in this figure has been reproduced from ref. 12. **b**, Representative images of c-Fos expression upon photostimulation of the injection sites shown in **a**. Coronal sections of the brains were stained for c-Fos (red) and EYFP (green), and counterstained with DAPI (blue). Scale bars, 100 μm. **c**, The percentage of $EYFP^+$ neurons co-expressing c-Fos upon photostimulation of the injection site ($n = 9$, 10, and 6 mice for wild-type animals injected with AAV_2-hSyn-EYFP, ChR2–EYFP, and NpHR–EYFP into S1DZ; 3 independent experiments). **d**, The number of $c\text{-}Fos^+$ cells in the contralateral hemisphere of the injection site for the animals described in **c**. **e**–**h**, The marble burying index (**e**), the percentage of interaction of the sociability test (**f**), the total interaction time of the sociability test (**g**), the time spent in the centre of an open field (**h**), and the total distance moved during the open field test (**i**) of animals prepared as in **a** (all during first laser-on test; $n = 9$, 12, and 10 for wild-type animals injected with AAV_2-hSyn-EYFP, ChR2–EYFP, and NpHR–EYFP into S1DZ; 3 independent experiments). $^*P < 0.05$, $^{**}P < 0.01$ calculated by two-way ANOVA with Tukey post hoc tests (**f**) and one-way ANOVA with Tukey post hoc tests (**c**, **d**, **e**, **g**, **h**, **i**). Graphs indicate mean ± s.e.m.

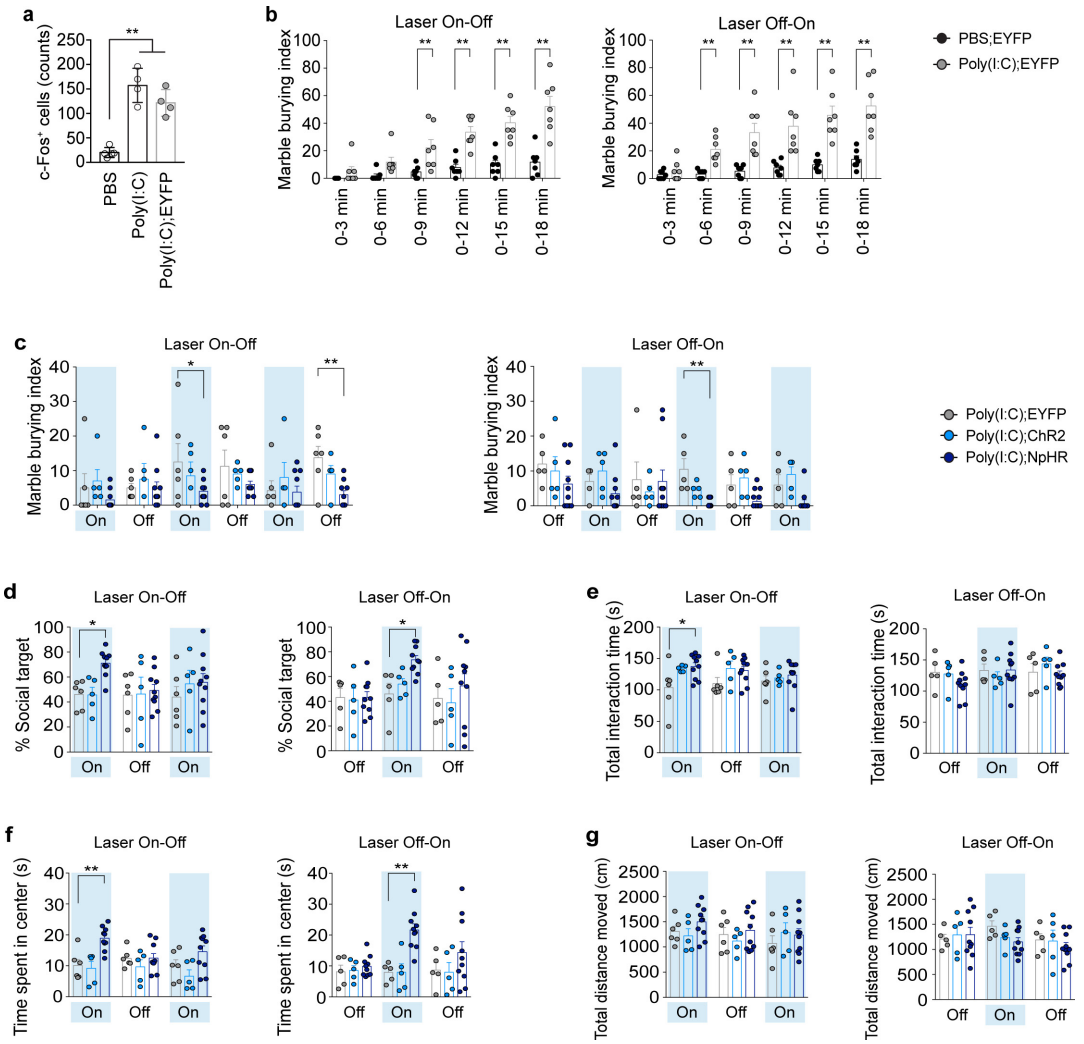

Extended Data Figure 10 | Reducing neural activity in the cortical region centred on the S1DZ corrects the behavioural abnormalities of MIA offspring. a, Quantification of c-Fos$^+$ cells in the S1DZ of adult offspring from mothers injected with PBS or poly(I:C), and of adult poly(I:C) offspring, in which AAV_2-hSyn-EYFP was injected into the S1DZ ($n = 5$, 4, and 4 mice for PBS, poly(I:C), and poly(I:C);EYFP groups, respectively; 3 independent experiments). **b**, AAV_2-hSyn-EYFP was targeted into the S1DZ of adult offspring from either PBS or poly(I:C) treated mothers. The accumulation of marble burying index over their behavioural session is plotted based on the laser schemes ('Laser On-Off': $n = 7$ and 7; 'Laser Off-On': $n = 7$ and 7 for AAV_2-hSyn-EYFP injected PBS and poly(I:C) offspring; 3 independent experiments, respectively). **c**–**g**, AAV_2-hSyn-EYFP, ChR2–EYFP, or NpHR–EYFP viruses were targeted to the S1DZ of MIA offspring (poly(I:C)). The marble burying index (**c**), the percentage of social target (**d**) and the total interaction time (**e**) of the sociability test, the time spent in the centre of an open field (**f**), and the total distance moved during the open field test (**g**) are plotted as averages from each individual 3-min session. Light blue indicates the laser 'On' sessions ('Laser On-Off': $n = 6$, 5, and 10; 'Laser Off-On': $n = 5$, 5, and10 for AAV_2-hSyn-EYFP, ChR2–EYFP, and NpHR–EYFP injected MIA offspring; 5 independent experiments). $^*P < 0.05$, $^{**}P < 0.01$ calculated by one-way ANOVA with Tukey post hoc tests (**a**) and two-way repeated measures ANOVA with Tukey post hoc tests (**b**, **c**, **d**, **e**, **f**, **g**). Graphs indicate mean ± s.e.m.

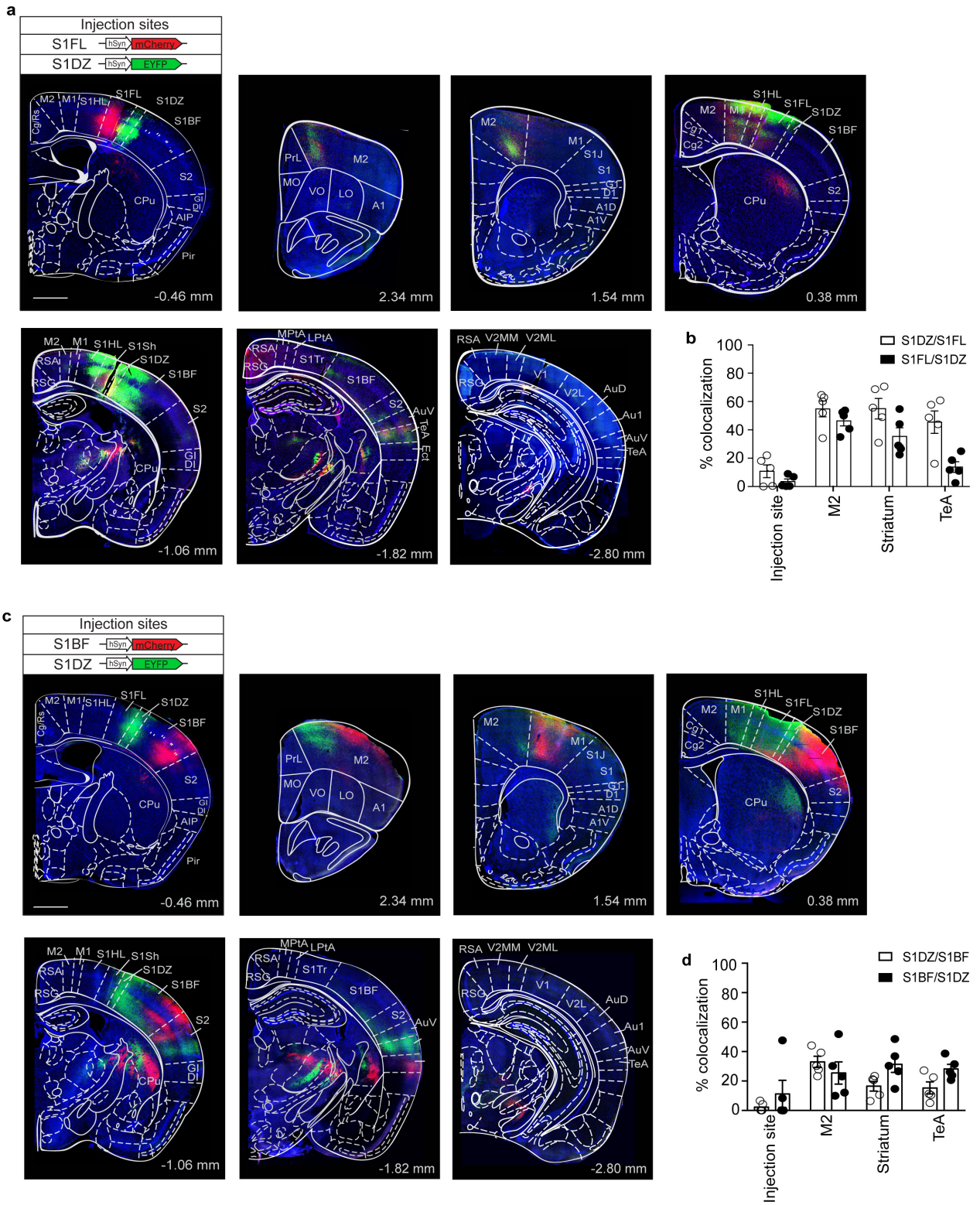

Extended Data Figure 11 | The S1FL, S1DZ, and S1BF exhibit distinct efferent targets. a, **c**, AAV_2-hSyn-mCherry and AAV_2-hSyn-EYFP were injected into the S1FL and S1DZ (**a**) or S1BF and S1DZ (**c**), respectively. The cortical regions project to distinct sub-regions of the M2, the striatum, and the associative cortices. Representative images are aligned to their corresponding AP levels in ref. 12 ($n = 5$). Scale bar, 1 mm. **b**, **d**, Quantification of percentage of co-localized projection fibres, represented as percentage (%) co-localization, from S1FL with those from S1DZ within the regions of interest (ROI; $n = 5$) (**b**) and from S1BF with those from S1DZ within the ROI ($n = 5$) (**d**). S1DZ/S1FL (S1DZ/S1BF) reflects the percentage S1FL (S1BF) projection fibres within the ROI co-localized with those from S1DZ, while S1FL/S1DZ (S1BF/S1DZ) reflects vice versa. The mouse brain in this figure has been reproduced from ref. 12. Graph indicates mean ± s.e.m.

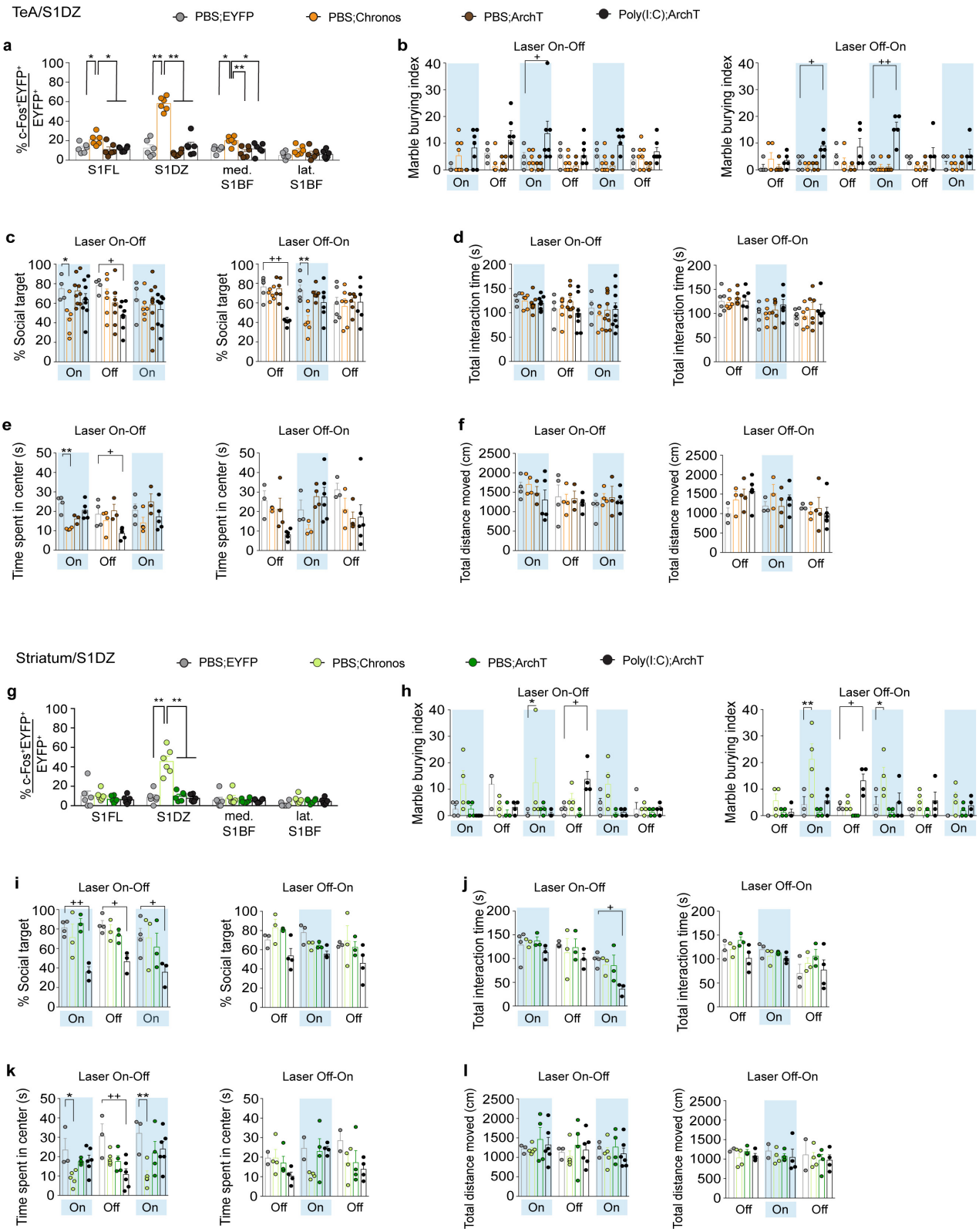

Extended Data Figure 12 | See next page for caption.

Extended Data Figure 12 | Distinct populations of S1DZ neurons projecting to TeA or striatum selectively modulate marble burying and sociability phenotypes. a, Percentage of EYFP and c-Fos co-expressing neurons upon stimulation of animals described in Fig. 5c ($n = 6, 6, 6, 6$ mice, 3 independent experiments (PBS; RV–EYFP, Chronos, ArchT, MIA; RV-ArchT)). **b–f**, Performance in the marble burying test (**b**) ('Laser On-Off': $n = 4, 8, 5, 7$ mice for PBS; EYFP, PBS; Chronos, PBS; ArchT, MIA; ArchT, 4, 7, 5, 7 independent experiments and 'Laser Off-On': $n = 5, 5, 5, 5$ mice for PBS; EYFP, PBS; Chronos, PBS; ArchT, MIA; ArchT, 5, 5, 5, 5 independent experiments), the percentage of social target (**c**) and the total interaction time during the sociability test (**d**) ('Laser On-Off': $n = 4, 6, 9, 9$ mice for PBS; EYFP, PBS; Chronos, PBS; ArchT, MIA; ArchT, 4, 5, 7, 7 independent experiments and 'Laser Off-On': $n = 6, 6, 6, 6$ mice for PBS; EYFP, PBS; Chronos, PBS; ArchT, MIA; ArchT, 5, 5, 5, 5 independent experiments), and the time spent in centre (**e**) and the total distance moved during the open field test (**f**) ('Laser On-Off': $n = 4, 4, 3, 5$ mice for PBS; EYFP, PBS; Chronos, PBS; ArchT, MIA; ArchT, 4, 4, 3, 5 independent experiments and 'Laser Off-On': $n = 3, 3, 4, 6$ mice for PBS; EYFP, PBS; Chronos, PBS; ArchT, MIA; ArchT, 3, 3, 4, 5 independent experiments). **g**, Percentage of EYFP and c-Fos co-expressing neurons upon stimulation of animals described in Fig. 5i ($n = 6, 6, 6, 6$ mice, 3 independent experiments (PBS; RV–EYFP, Chronos, ArchT, MIA; RV-ArchT)). **h–l**, Performance in the marble burying test (**h**) ('Laser On-Off': $n = 4, 4, 4, 4$ mice for PBS; EYFP, PBS; Chronos, PBS; ArchT, MIA; ArchT, 4 independent experiments and 'Laser Off-On': $n = 3, 4, 4, 4$ mice for PBS; EYFP, PBS; Chronos, PBS; ArchT, MIA; ArchT, 3 independent experiments), the percentage of social target (**i**) and the total interaction time during the sociability test (**j**) ('Laser On-Off': $n = 4, 3, 3, 3$ mice for PBS; EYFP, PBS; Chronos, PBS; ArchT, MIA; ArchT, 3 independent experiments and 'Laser Off-On': $n = 3, 3, 3, 4$ mice for PBS; EYFP, PBS; Chronos, PBS; ArchT, MIA; ArchT, 3 independent experiments), and the time spent in centre (**k**) and the total distance moved during the open field test (**l**) ('Laser On-Off': $n = 3, 5, 4, 6$ mice for PBS; EYFP, PBS; Chronos, PBS; ArchT, MIA; ArchT, 3, 5, 4, 5 independent experiments and 'Laser Off-On': $n = 2, 4, 4, 4$ mice for PBS; EYFP, PBS; Chronos, PBS; ArchT, MIA; ArchT, 2, 4, 4, 4 independent experiments). *,$^{+}P < 0.05$, **, $^{++}P < 0.01$ calculated by one-way ANOVA with Tukey post hoc tests (**a**, **g**) and two-way repeated measures ANOVA with Tukey post hoc tests (**b–f**, **h–l**). Graphs indicate mean ± s.e.m.

nature research

Corresponding author(s): Jun Huh

☐ Initial submission ☐ Revised version ☒ Final submission

Life Sciences Reporting Summary

Nature Research wishes to improve the reproducibility of the work that we publish. This form is intended for publication with all accepted life science papers and provides structure for consistency and transparency in reporting. Every life science submission will use this form; some list items might not apply to an individual manuscript, but all fields must be completed for clarity.

For further information on the points included in this form, see Reporting Life Sciences Research. For further information on Nature Research policies, including our data availability policy, see Authors & Referees and the Editorial Policy Checklist.

Experimental design

1. Sample size

Describe how sample size was determined.

Sample sizes were estimated based on similar, previously-conducted studies (page 33).

2. Data exclusions

Describe any data exclusions.

Behavioral results from mice without viral infection or with inaccurate targeting of virus of fiber implantations were excluded (page 27). Cortical regions that had (1) weak SATB2 or TBR1 expression or (2) displayed tissue damage were not considered as cortical patches (page 31).

3. Replication

Describe whether the experimental findings were reliably reproduced.

Key experiments, including the location of cortical patches, anterograde tracing experiments, and behavioral experiments with optical modulation, were all independently repeated with similar observations (page 33).

4. Randomization

Describe how samples/organisms/participants were allocated into experimental groups.

Animals were randomized into different groups with approximately comparable numbers of animals in each group whenever possible (page 33).

5. Blinding

Describe whether the investigators were blinded to group allocation during data collection and/or analysis.

For behavior, immunohistochemistry, and postsynaptic current analysis, experimenters were blind to the treatment group (page 24,27,29,32).

Note: all studies involving animals and/or human research participants must disclose whether blinding and randomization were used.

6. Statistical parameters

For all figures and tables that use statistical methods, confirm that the following items are present in relevant figure legends (or in the Methods section if additional space is needed).

n/a	Confirmed
☐	☒ The exact sample size (*n*) for each experimental group/condition, given as a discrete number and unit of measurement (animals, litters, cultures, etc.)
☐	☒ A description of how samples were collected, noting whether measurements were taken from distinct samples or whether the same sample was measured repeatedly
☐	☒ A statement indicating how many times each experiment was replicated
☐	☒ The statistical test(s) used and whether they are one- or two-sided (note: only common tests should be described solely by name; more complex techniques should be described in the Methods section)
☐	☒ A description of any assumptions or corrections, such as an adjustment for multiple comparisons
☐	☒ The test results (e.g. *P* values) given as exact values whenever possible and with confidence intervals noted
☐	☒ A clear description of statistics including central tendency (e.g. median, mean) and variation (e.g. standard deviation, interquartile range)
☐	☒ Clearly defined error bars

See the web collection on statistics for biologists for further resources and guidance.

Software

Policy information about availability of computer code

7. Software

Describe the software used to analyze the data in this study.	SAS Prolab software (page 25) was used for ultrasonic vocalization (USV) analysis, while EthoVision tracking system (page 25-27) was used for sociability and open field assay analysis.

For manuscripts utilizing custom algorithms or software that are central to the paper but not yet described in the published literature, software must be made available to editors and reviewers upon request. We strongly encourage code deposition in a community repository (e.g. GitHub). *Nature Methods* guidance for providing algorithms and software for publication provides further information on this topic.

Materials and reagents

Policy information about availability of materials

8. Materials availability

Indicate whether there are restrictions on availability of unique materials or if these materials are only available for distribution by a for-profit company.	N/A

9. Antibodies

Describe the antibodies used and how they were validated for use in the system under study (i.e. assay and species).	Anti-rabbit-TBR1 (ab31940, Abcam, USA), anti-mouse-SATB2 (ab51502, Abcam, USA), anti-rabbit-PV (PV27, Swant, Switzerland), anti-rabbit-VIP (20077, Immunostar, USA), anti-mouse-NeuN (MAB377X, Millipore, USA), and anti-rabbit-c-Fos (sc-7270, Santa Cruz, USA; ABE457, Millipore, USA) antibodies were used for immunohistochemical analysis in this study (page 29).

10. Eukaryotic cell lines

a. State the source of each eukaryotic cell line used.	N/A
b. Describe the method of cell line authentication used.	N/A
c. Report whether the cell lines were tested for mycoplasma contamination.	N/A
d. If any of the cell lines used are listed in the database of commonly misidentified cell lines maintained by ICLAC, provide a scientific rationale for their use.	N/A

Animals and human research participants

Policy information about studies involving animals; when reporting animal research, follow the ARRIVE guidelines

11. Description of research animals

Provide details on animals and/or animal-derived materials used in the study.	C57BL/6 mice were purchased from Taconic (USA), and Nestin-cre (003771), PV-cre (008069), and vGluT2-cre (016963) mice from Jackson laboratory (USA). IL-17Rafl/lfl mice were obtained as described previously (page 22).

Policy information about studies involving human research participants

12. Description of human research participants

Describe the covariate-relevant population characteristics of the human research participants.	N/A